Chapter 3

Adsorption of Chromium from aqueous solutions using Zirconium Phosphate modified Chitosan

3.1 Introduction

The metal salts of phosphoric acid are well known. Zirconium bis-(monohydrogen orthophosphate) monohydrate ($Zr(HPO_4)_2H_2O$), also called layered α-zirconium phosphate (ZrP), is drawing increasing attention due to its ability to serve as an ion exchanger, catalyst and also to its ability to intercalate (Cai et al., 2012; Karlsson, Andersson, & Hjortkjaer, 2001). The layers (where the interatomic interaction is essentially covalent) connected by weak van-der Waals forces, result in two-dimensional materials which allow other species (atoms, ions or molecules) to penetrate into the interlayer space. (Jaimez, Khainakov, Trobajo, & Rodrı, 1998; Trobajo et al., 2001). The layered structure of α-Zirconium Phosphate (ZrP) consists of zirconium ions in a semiplanar arrangement, located slightly above and below the mean plane, while each of the Zr^{4+} ions is connected through the oxygen atoms of phosphate groups above and below the zirconium atom plane. Each of the three oxygens of a phosphate group is bonded to a different zirconium, resulting in one free -OH group, pointing to the inter layer region. These P-OH groups are responsible for α-ZrP Bronsted acidity, Fig. 3.1.

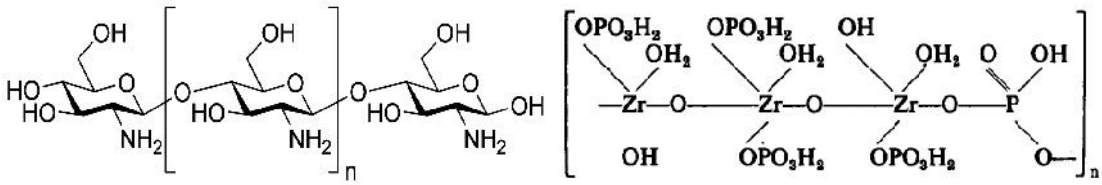

Figure 3.1 Structure of CH and ZrP

Hence, each of the Zr^{4+} ions is octahedrally coordinated by six oxygens of six different phosphate groups (A Clearfield & Stynes, 1964; Abraham Clearfield & Smith, 1969; Sun, Boo, Browning, Sue, & Clearfield, 2005; Troup & Clearfield, 1977; F. Zhang et al., 2010).

Further due to its lamellar structure and abundant hydroxyl groups, ZrP has high ion exchange capability, excellent adsorptive potential and can thus be functionalized. In recent years, layered zirconium phosphate has thus been recognized for its wide range of applications (Swain et al., 2011; Takei et al., 2006). The stability and strong resistance of ZrP

to acid and alkali further broaden its application scope (Pica et al., 2011). Furthermore, through the ionic bonds, van-der Waals force and hydrogen bonds, the layered structure can be inserted or grafted with special organic groups into the third dimension, which allows to control interlayer distances, selectivity, absorption capacity and reactivity (Kumada et al., 2011; Q. Zhang et al., 2011). Therefore, this material shows immeasurable potential and increasing importance in catalysis (Calogero et al., 2011), Adsorption (Swain et al., 2011; Q. Zhang et al., 2011) and proton conductivity (Nishiyama et al., 2006).

In particular, several studies had been done on the use of zirconium phosphate adsorbents, such as amorphous zirconium phosphate (B. Pan et al., 2007), Microporous zirconium phosphate (Mao, Wang, & Clearfield, 2002) and Nanosized zirconium phosphate (L. Wang et al., 2013).

Several researchers (Chourasia, Bohre, Shrivastava, & Wattal, 2010; Q. Zhang et al., 2013; Dan Zhao, Li, Zhang, Yang, & Zhu, 2011) have observed that Zr phosphate and Zr oxide had high phosphate adsorption capacity. However, the drawback of these materials for practical applications is due to their microcrystalline nature and their occurrence as fine-grained powders: the recovery of the sorbent (solid/liquid separation) in batch system or the hydrodynamic properties of fixed bed systems are the limiting criteria (pressure head loss, column blockage, sluggish flow rates, etc.). These problems may be circumvented by (a) immobilizing the inorganic ion-exchangers on oxide supports (Sydorchuk, Khalameida, Skubiszewska-Zieba, & Leboda, 2011), such as silica (Chang, Chau, Hu, Wang, & Liao, 2008), alumina (Chakravarty et al., 2012; Satyanarayana, Murthy, & Sasidhar, 1999) or (b) encapsulating these materials in synthetic polymers (Cabatingan, Agapay, Rakels, Ottens, & van der Wielen, 2001; Chauhan, Jaiswal, & Sankararamakrishnan, 2012; Hepplewhite, Newcombe, & Knappe, 2004; Nilchi, Zarghami, Saberi, Moradi, & Azizpour, 2012; B. C. Pan et al., 2007; Rudzinski & Panczyk, 2002; Tranter, Herbst, & Todd, 2002; Q. Zhang, Jiang, Pan, Zhang, & Lv, 2009) or biopolymers (Elovich & Larionov, 1962; Mimura et al., 2011). The challenge then consists in managing simultaneously the confinement of the reactive mineral sorbents without sacrificing mass transfer properties (kinetics and accessibility to reactive sites).

A hierarchical porous zirconium phosphate membrane was prepared by Abutartour et al. from bis(hexamethylene triaminepenta (methylenephosphonic acid)), $ZrOCl_2 8H_2O$, SiF_4 and hexadecyl trimethyl ammonium bromide. The membrane contains macropores of 200 nm in diameter and mesopores of 19.2 nm in diameter. The membranes pores were bridged and

limited by (-Si-O-)n edges. The porous membrane exhibited high efficiency in removing Pb^{2+} and Cu^{2+} from wastewater (Abutartour, Jia, Majdoub, & Xu, 2014).

In recent years, some zirconium phosphate hybrid materials were reported, which include polymer-supported zirconium phosphate (B. Pan et al., 2006) and zirconium phosphate silica gel (Matoso, Kubota, & Cadore, 2003). Zirconium phosphate modified polyvinyl alcohol (PVA)-PVDF membrane was developed for lead removal (Dandan Zhao, Yu, & Chen, 2016). The zirconium ions and PVA were initially coated onto a PVDF membrane by crosslinking with glutaraldehyde and then modified by phosphate.

Recently, the nanocomposite ion exchangers consisting of organic conducting polymers and inorganic ion-exchange materials such as ZrP have been considered as the ideal adsorption materials for ion selective separation (Pathania, Sharma, & Thakur, 2015). Such hybrid materials combine the good conductivity and film-forming ability of conducting polymers and the high ion exchange capacity and selectivity of inorganic materials.

ZrP-pillared rGO (reduced graphene oxide) was prepared which was employed as the adsorbent towards methylene blue (Z. Wu, Zhang, Guan, Ning, & Ye, 2014). Krys et al. encapsulated, two mineral sorbents, ammonium molybdophosphate (AMP) and hydrogen zirconium phosphate (Phozir), (alone or in combination) in a biopolymer matrix made of alginate for the sorption of rubidium (Krys et al., 2013).

Zirconia is a biologically inert material and has good biocompatibility with chitosan. Even if Zr modified chitosan was inefficiently recovered after being used as adsorbent, the good biocompatibility will significantly decrease the secondary contamination to environment. Recently, Zr^{4+} modified chitosan (or chitosan derivatives) has been investigated for the removal of phosphate from aqueous solution which include Zr^{4+} loaded cross-linked chitosan beads (X. Liu & Zhang, 2015), Zr^{4+} modified chitosan beads (Sowmya & Meenakshi, 2014), Zr^{4+} loaded cross-linked chitosan (CCP-Zr) prepared by membrane-forming and cross-linking (Q. Liu, Hu, Wang, Zhang, & Huang, 2016) and nanocomposite Fe_3O_4/ZrO_2/chitosan (Jiang et al., 2013).

Zirconium pillared Mt (Zr-Mt) was used as adsorbent to remove Cr^{3+} by Hei et al. (Hei & Ma, 2016). Guerra et al. further reported that the adsorption capacity of Zr-Mt is better than that of Zr/Al-Mt (Jiang et al., 2013). Phosphate-immobilized zirconium pillared clay was effective in removing Hg^{2+}, Cd^{2+} and Co^{2+} effectively (Anirudhan, Bringle, & Radhakrishnan, 2012). Ma et al. developed zirconium-pillared montmorillonite (Zr-Mt) porous ceramic (P-ZMt) for Cr^{3+} removal by gelcasting (Ma et al., 2016a). Maltez et al.

explored the potential of silica gel modified with zirconium for chromium speciation by atomic spectrometry. In this study Cr^{6+} and Cr^{3+} sample was passed sequentially through silica gel modified with zirconium phosphate (SiO_2-ZrP) and silica gel modified with Zr^{4+} oxide (SiO_2-Zr). The SiO_2-ZrP retains positively charged Cr species and the SiO_2-Zr retains negatively charged Cr species (Maltez & Carasek, 2005).

Since chitosan is known to reduce Cr^{6+} to Cr^{3+} it was felt that chitosan modified ZrP(CZrP) could be used to remove Cr^{6+} and Cr^{3+} as Cr^{3+} has inherent affinity towards ZrP. The hypothesis was explored in this study.

3.2 Materials and Methods.

3.2.1 Materials

All the reagents used were of AR grade, stock and working solutions of Cr^{6+} were prepared by dissolving $K_2Cr_2O_7$(AR grade) in deionized double distilled water. Chitosan from Crab cells (Sigma Aldrich, USA) and $ZrOCl_2.8H_2O$ from Loba chemicals & H_3PO_4 from Merck Chemicals. For Adsorption study, Chitosan-Zirconium Phosphate composite used as adsorbent.

3.2.2 Synthesis of CZrP

3.2.2.1 Synthesis of ZrP

A sample of 4 g of $ZrOCl_2.8H_2O$ was mixed with 40 ml of 5 M H_3PO_4 which was sealed and kept in an autoclave for three hours and pressure was maintained at 15 psi. The obtained white product was centrifuged and washed with deionised water till 7 pH was obtained and then dried at 50^oC (Abutartour et al., 2014).

3.2.2.2 Synthesis of Chitosan modified with ZrP

To 1% CH solution (in 1% Acetic Acid), 0.5% of ZrP (w/v in water) was mixed and kept in stirring condition for 24 hrs. A white material CZrP was formed which was then filtered, washed with double distilled water to neutral and dried overnight in vacuum oven at 30°C. The material was then crushed well and its potential as adsorbent was investigated.

3.2.3 Preparation of metal solutions

Stock Solution Prepared as per 2.2.3 of Chapter 2

3.2.4 Batch sorption Experiments

Batch sorption done as per 2.2.4 of Chapter 2

3.2.5 Equilibrium Sorption Studies

Equilibrium Sorption Studies were explained as per 2.2.5 of Chapter 2 with CZrP.

3.2.6 Sorption Dynamics

Sorption Dynamics explained as per 2.2.6 of Chapter 2 with CZrP.

3.2.7 Thermodynamics of Sorption Studies

Thermodynamics Studies explained as per 2.2.7 of Chapter 2 with CZrP

3.2.8 Characterization techniques

Characterization done as per 2.2.8.1 to 2.2.8.11 of Chapter 2

3.2.9 Desorption

For desorption studies, 0.05 g of CZrP preloaded with Cr^{6+} was equilibrated with 25 ml solutions of 0.1 M of NaOH, H_2SO_4, HCl and HNO_3 for 120 min. The contents of the flasks were filtered and the chromium content in the filtrate was determined by ICP. Three consecutive adsorption-desorption cycles were carried out to test the reusability of CZrP.

3.3 Results and discussion

3.3.1 Zeta potential

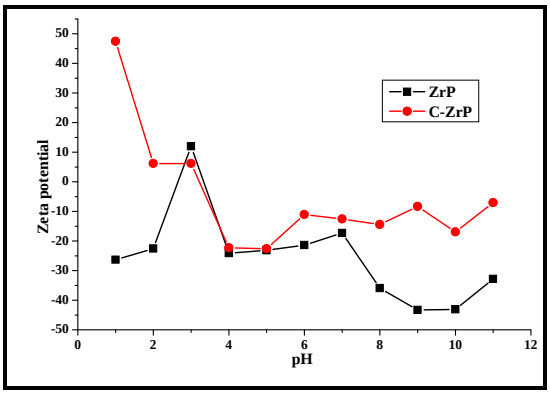

Figure 3.2 Zeta Potential of CZrP

The α-Zrp particles show a strong negative zeta potential (Figure 3.2), where as chitosan as a cationic polyelectrolyte shows a very strongly positive zeta potential at acidic pH suggesting a strong electrostatic attraction amenable for the formation of the composite. The zeta potential increased from -30 to + 50 at pH 1and decreased from -10 to -45 at pH 9 for Zrp to C ZrP (Waraich, 2012). The zpc value was found to be at pH 3.8.

3.3.2 Elemental and Surface area Analysis

The elemental composition of the sample measured by microanalysis and SEM EDAX are tabulated in Table 3.1 and the SEM images are shown in Figure 3.3.

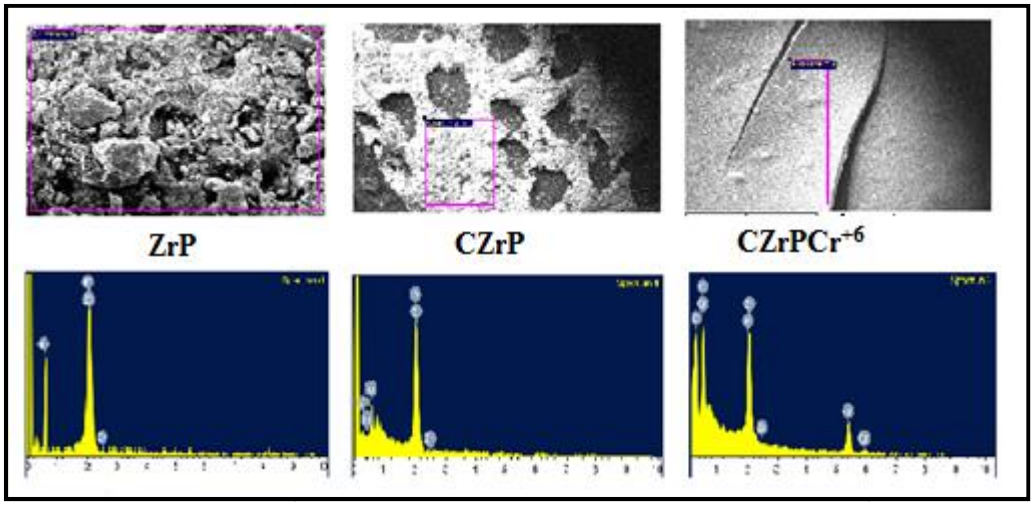

Figure 3.3 SEM / EDAX a) ZrP b) CZrP and c) CZrPCr

Table 3.1 CHN microanalysis

	ZRP			**CZrP**			**CZrPCr^{6+}**		
Element	Weight%	Atomic%	CHN	Weight%	Atomic%	CHN	Weight%	Atomic%	CHN
Carbon				18.2	29.55	7.66	38.83	51.34	7.75
Nitrogen				2.28	3.17	1.22	1.12	1.55	1.25
Hydrogen			1.64			1.9			2.13
Zirconium				20.05	4.29		6.39	1.11	
Phosphorus				16.13	10.16		5.39	2.76	
Oxygen				43.34	52.84		42.10	41.35	
Chromium							6.16	1.88	

Figure 3.3 showed the EDX spectrum of ZrP, indicating that ZrP contained elements of O, P and Zr, which meant it was a $Zr(HPO_4)_2H_2O$. From Figure 3.3, the flaky and amorphous nature of chitosan is observed as well as the nano particle nature of the synthesized ZrP. It is seen that ZrP is uniformly distributed in the chitosan matrix in CZrP. The EDAX data confirms the modification of chitosan with ZrP and adsorption of chromium onto ZrP.

The surface area of the ZrP obtained from N_2 adsorption−desorption study was found to be 3.3740 m^2/g. A pore size of 100.1561 Å corresponding to a maximum pore volume of 0.00434 cm^3/g was obtained from the Barrett-Joyner-Halenda (BJH) pore size distribution curve while the surface area of CZrP obtained from N_2 adsorption−desorption study was found to be 33.7067 m^2/g with a pore size of 168.5680 Å corresponding to a maximum pore volume of 0.10186 cm^3/g .

3.3.3 TEM analysis

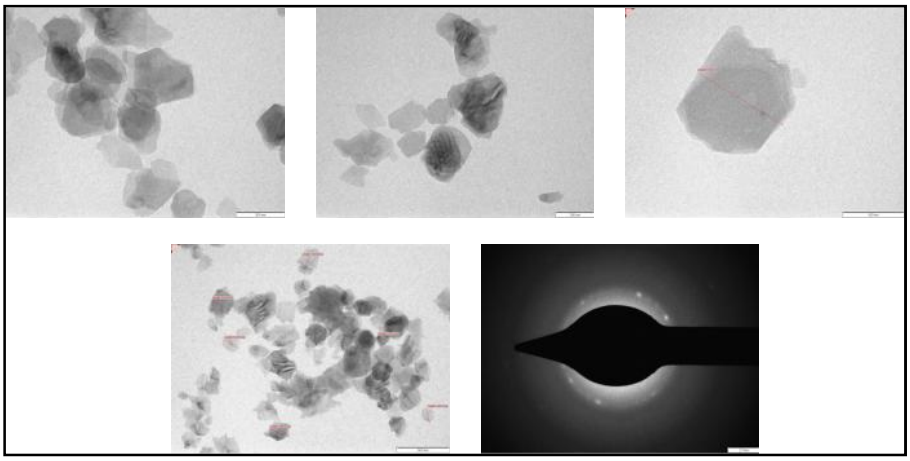

Figure 3.4 TEM a) ZrP

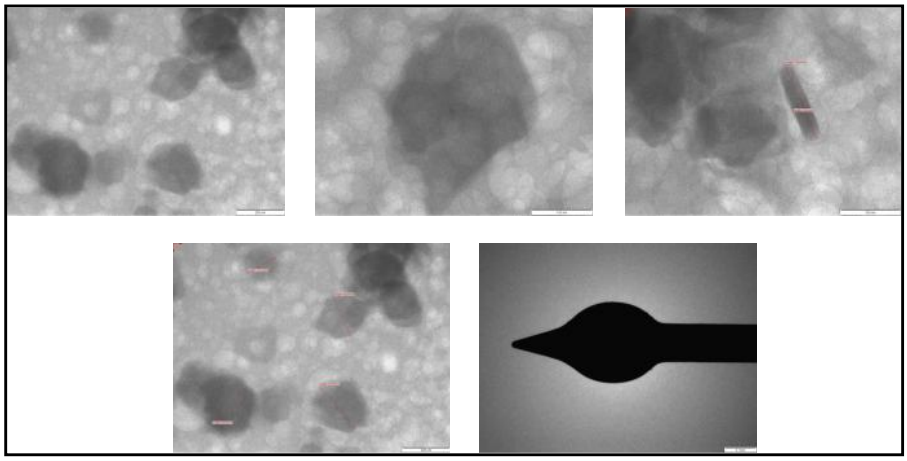

Figure 4.4 TEM b) CZrP

Figure 3.4 shows the TEM images in ZrP as layers of hexagonal platelets of size 180nm and some irregularly shaped sheets are stacked one upon another and CZrP clearly shows ZrP of size ~60 nm platelets and ~136nm rods uniformly distributed in the chitosan matrix. The SAED pattern of ZrP show that ZrP is partly crystalline in nature while crystallinity is almost lost in CZrP.

3.3.4. FTIR Analysis

Figure 3.5 shows the IR spectra of ZrP, C-ZrP and Cr-CZrP. The FTIR data of α-ZrP shown the intense broad characteristic peak at ~1050 cm^{-1} assigned to symmetrical stretching vibration of PO_4^{3-} (Q. Zhang et al., 2013). The peaks at 1251 cm^{-1} can be attributed to P-OH stretching or deformation vibrations of HPO_4^{2-}. The peaks at 3595, 3518, 3151 and 1619 cm^{-1} were attributed to the symmetric and asymmetric stretching and bending vibrations of water in ZrP. Spectra showed band located at 596 cm^{-1} in ZrP that can be assigned to Zr-O bonds.

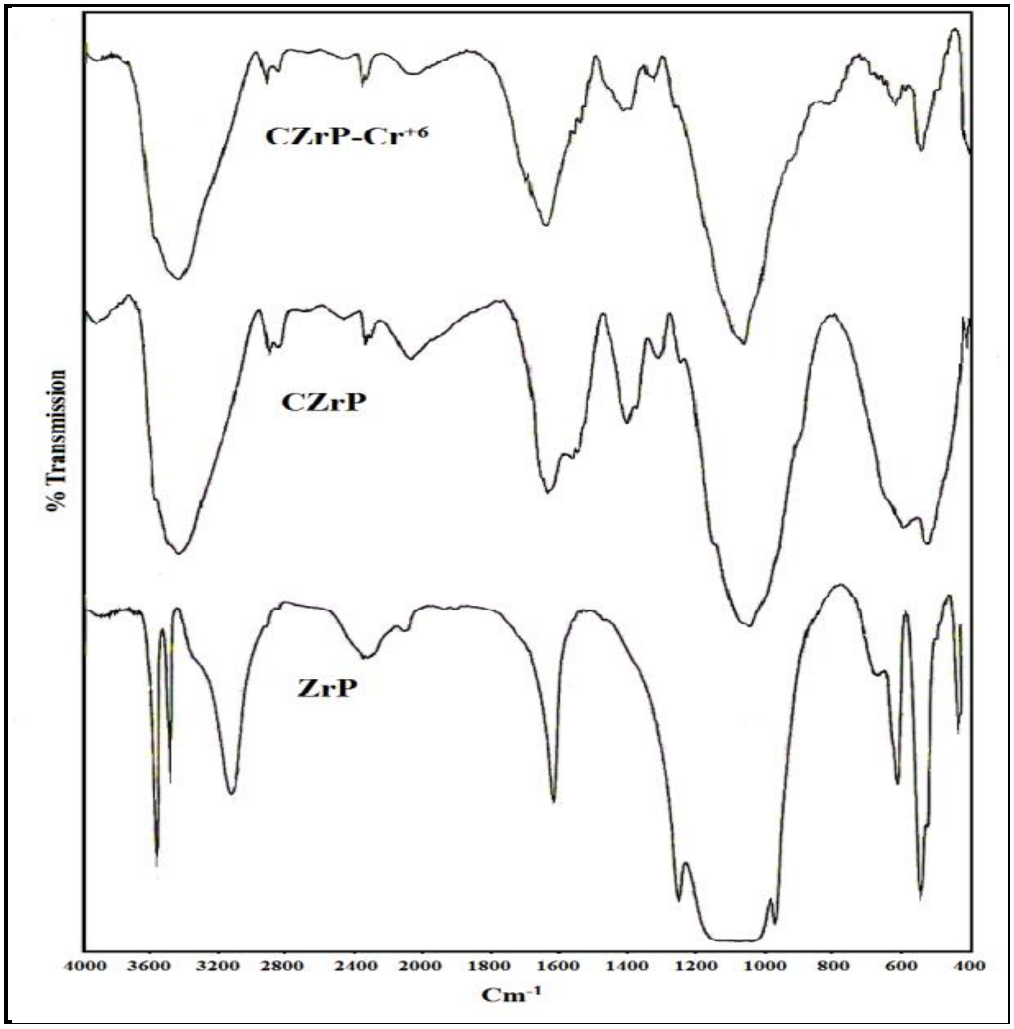

Figure 3.5 FTIR Spectra of a) ZrP b) CZrP and c) CZrPCr

Chitosan shows characteristic FTIR peaks in the range of 1500 to 1690 cm^{-1} which can be attributed to primary amino group (-N-H). The band at 1546 cm^{-1} can be attributed to C-H bending. The band in the range 1050 to 1393 cm^{-1} is due to C-O bending and peak at 3619 cm^{-1} is due to stretching of free hydroxyl groups in chitosan. The broad band at 2857 cm^{-1} is due to aldehydic (H-C=O) stretching vibrations.

Absorption at 1051 cm^{-1} is due to C-N stretching mode of chitosan. IR band at 524 and 604 cm^{-1} is also due to Zr-O-C stretching mode. Thus FTIR data supported complete dispersion of Zirconium phosphate into chitosan (Dongre, Ghugal, Meshram, & Ramteke, 2012). It is observed that the FTIR band at 1643 cm^{-1} attributed to vibrational mode of C=O group of amide linkage in C-ZrP gets shifted by 12 cm^{-1} after chromium adsorption.

Table 3.2: Absorption and stretching frequencies of ZrP, CZrP and Cr^{+6} loaded CZrP

Chitosan	ZrP	CZrP	Cr^{+6} loaded CZrP	Inference
3859, 3747, 3619,3420	3595, 3518, 3151	3452	3442	O-H, N-H Stretching vibration
2929, 2857	-	2925	2929	aliphatic–CH stretching vibration
1697				N-H bend
1650		1643	1631	polypeptide amide I and C=O stretching vibrations
-	1619	1601		bending vibrations of –OH of water associated with PO_4^{3-} group
1546, 1502	1498	1550		polypeptide amide II(NH bending)and C-N stretching
1457	-	-	-	NH_3^+
,1393	-	1409,	1404	–CH symmetric bending vibrations in –CHOH
1051	-	-	-	–C-N stretching vibration
	1251,	1362		P-OH stretching
		1316	1315	OH stretching vibration
	1099	1045	1047	Symmetrical stretching vibration of phosphate
671	644	622		Asymmetric C-H bending vibration
-	-	-	521	Cr–O stretching Vibration
	533	524		Zr-O stretching
542	596	604	598	O-H out of plane bend, Zr-O-C stretching

(Du et al., 2016; Kousalya, Rajiv Gandhi, & Meenakshi, 2010; X. Liu & Zhang, 2015; J. S. Wang, Peng, Yang, Liu, & Hu, 2011; Zuo & Balasubramanian, 2013)

3.3.5 Raman Analysis

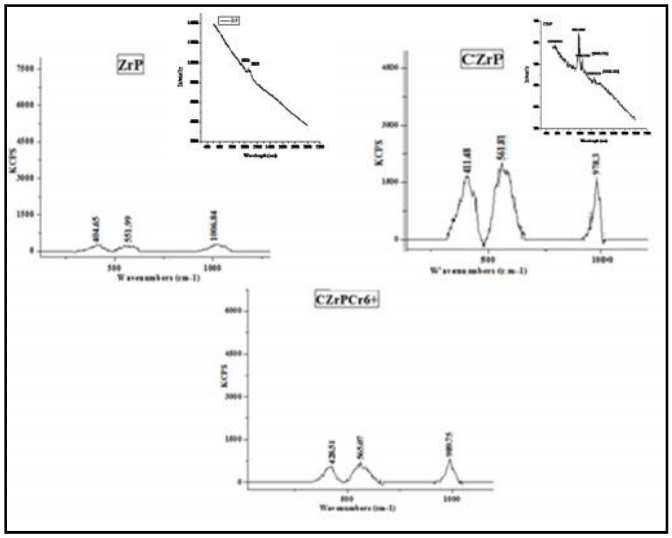

Figure 3.6 Raman Spectra of ZrP, CZrP and CZrPCr+6

Table 3.3: Raman frequencies for ZrP and CZrP

Samples	**Wave numbers (cm^{-1})**	Interpretation
ZrP	404.65	Symmetric bending PO_4^{3-}
	551.99	Zr-O stretch
	1006.84	ν3(PO_4) stretching
	1050, 1079	Stretching vibration of P-O
CZrP	411.48	Symmetric bending PO_4^{3-}
	561.81	Zr-O stretch
	978.	ν3(PO_4) stretching
	957	phosphate scissors and bond length vibrations
	1050	Stretching vibration of P-O
	1250	Δ(OH) out of plane
$CZrPCr^{6+}$	428.51	Symmetric bending PO_4^{3-}
	565.07	Zr-O stretch
	989.75	ν3(PO_4) stretching

The bands are more sharp and intense in ZrP than CZrP. It could be due to surface enhancement of raman signal (SERS) due to chitosan. There is a shift and weakening of peak of P-O probably due to replacement with chromium and we further note that the frequencies of the antisymmetric ν3(PO_4) stretching band at 1006.84 cm^{-1} is shifted to slightly higher frequencies at 978 and 989 cm^{-1} respectively for CZrP and CZrPCr indicating a slight shortening of the P–O bonds, i.e. a decrease of the volume of the PO_4 tetrahedron. The Raman spectra showed bands at 551.99, 561.81, 565.07 cm^{-1}respectively for ZrP, CZrP and CZrPCr. assigned to bridging-hydroxy group perpendicular-to-plane Zr–O stretch (He et al., 2016).

Free Cr^{6+} ion in 0.5 mol/l of potassium dichromate solution has a characteristic peak at 903.3 cm^{-1} (Ren et al., 2016). Weckhuysen et al. reported that Raman peaks for chromium compounds were located between 800 and 1030 cm^{-1} (Weckhuysen & Schoonheydt, 1999). Chowdhury also observed a new Raman peak at 826.4 cm1 in Cr^{6+} laden maghemite–magnetite nanoparticles (Chowdhury, Yanful, & Pratt, 2012).

3.3.6 TGA and DSC

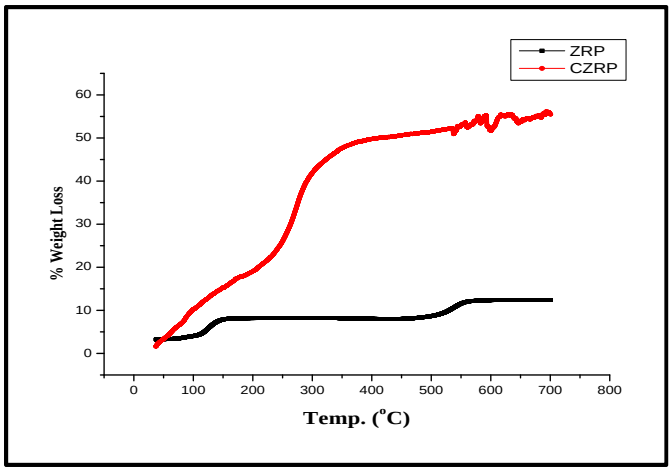

Figure 3.7 TGA of a) ZrP and b) CZrP

The TGA curves of ZrP and CZrP are shown in Figure 3.7. The TGA thermogram obtained for α-ZrP shows two major weight losses (centered around 150° and 550° C, respectively), with a total loss of ca. 9% indicating significant thermal stabilities of ZrP particles. As reported by Mosby et al. these weight losses could be attributed to complete dehydration and condensation of the phosphate groups producing zirconium pyrophosphate (Mosby, Díaz, Bakhmutov, & Clearfield, 2014). ZrP showed higher weight loss due to loss of water (11%) at 125°C which was lesser for C-ZrP (2%)suggesting significantly less water in CZrP. The second weight loss seen in C- ZrP at 300°C corresponds to the dehydration of the saccharide rings and depolymerization (Mathew & Dufresne, 2002), i.e deacetylation and degradation of chitosan.. The thermal stability of C-ZrP is found to be lower than that of ZrP. This could be attributed to the increase in acidity of α-ZrP with the increase in temperature, which induces the decomposition of the glycoside bonds (H. Wu et al., 2009). However, the weight loss is less. The thermal degradation temperature of chitosan was improved due to the fact that the ZrP nanolayers were well dispersed in chitosan in CZrP.

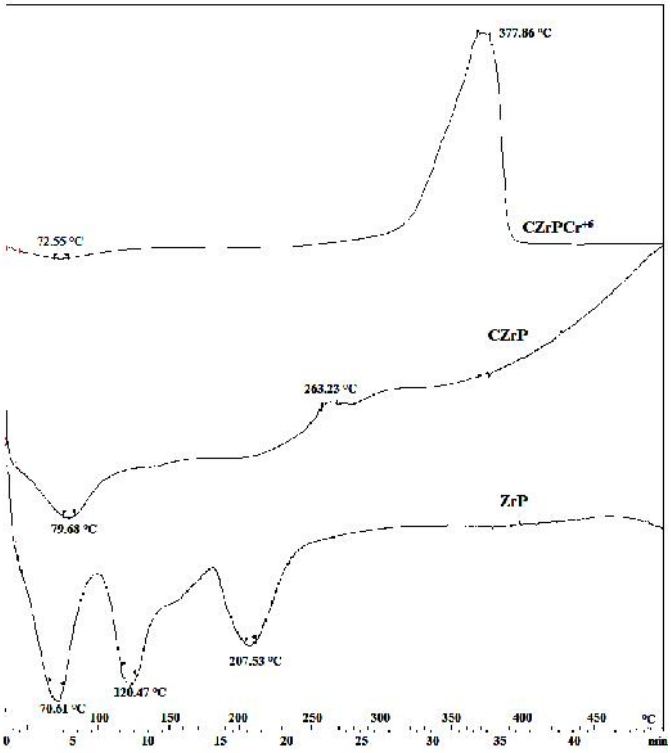

Figure 3.8 DSC a) ZrP, b) CZrp and c) $CZrpCr^{6+}$

From Figure 3.8, the endothermic peaks at 70.61°C and 120.47°C are attributed to evaporation of water associated with ZrP by different kinds of physical bonds (H-bonds, electrostatic interactions) in their interlayers and surface while decomposition was observed at 207.53°C. In CZrP the endothermic peak attributed to evaporation of water was observed at 79.68°C while exothermic peak at 263.23°C can be attributed to deacetylation of chitosan in C-ZrP suggesting that pillaring of ZrP onto chitosan was inhibiting crystallisation. In contrast in Cr-CZrP the dehydration step was observed as a small endothermic peak at 72.5°C followed by a decomposition step with intense exothermic effect at 377.86°C.

3.3.7 XRD Analysis

The strong diffraction peaks at 11.71°, 19.8°, 24.9° and 34.06 corresponded to the characteristic diffraction peaks of α-$Zr(HPO_4)_2 \cdot H_2O$ at (002), (110), (112), and (020) planes respectively (JCPDS no. 33-1482) (Yan-Qing, Zhao-Jia, & Ming-Lin, 2015). The typical diffraction peak at 11.71° corresponded to a basal spacing (002) of 0.766 nm. Similar basal spacing was observed by several researchers (Murray, 2006; Z. Wu et al., 2014). The XRD pattern of CZrP shown in Figure 3.9 demonstrates that the layered structure of α-Zrp and crystallinity of the material is considerably retainable though less in CZrP and also after adsorption of Cr.

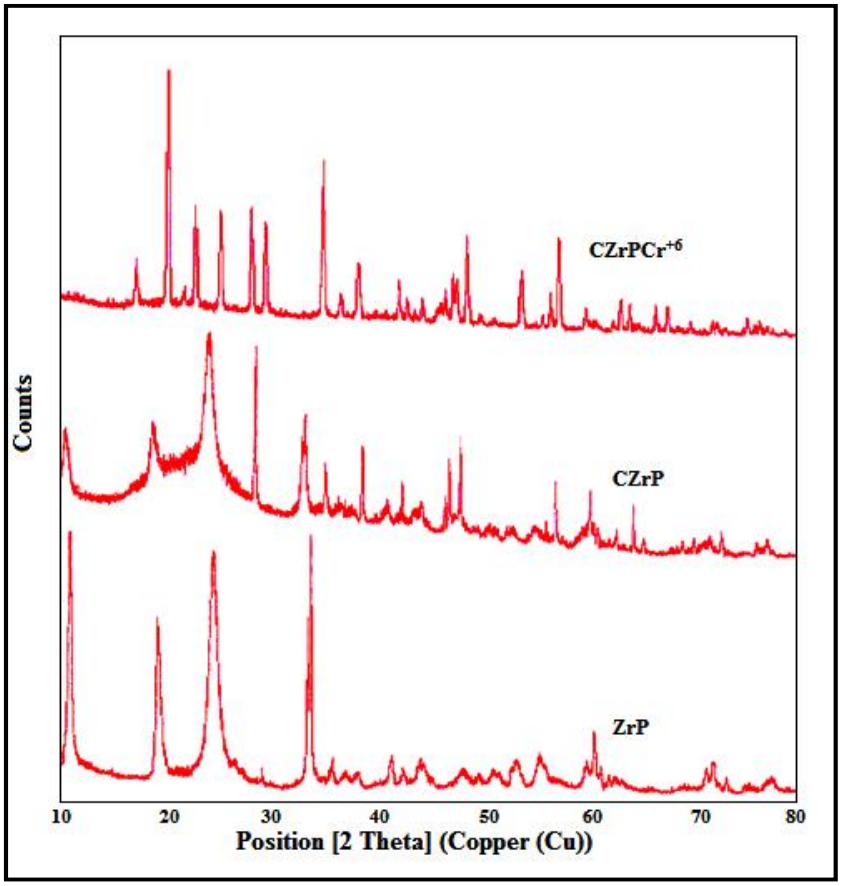

Figure 3.9 XRD a) ZrP b) CZrP and c) CZrPCr

As shown in Figure 3. 9, CZrP demonstrated a major reflection approximately 2 θ = 20°, which is representative of the crystallinity of form II (H. Zhao, Li, Li, Qiao, & Xu, 2015) of chitosan. In contrast, Cr-CZrP (Figure 3.9) did not show significant peak at 2θ = 20°, indicating that the ordered crystalline structure of CZrP has been slightly decreased by adsorption of chromium (Hosseini, Rezaei, Zandi, & Farahmandghavi, 2015). XRD studies(Chaper 2 section 2.3.7) show that pristine chitosan itself is amorphous in nature (Zhu, Jiang, Xiao, & Zeng, 2010) The X-Ray diffraction peaks for ZrP were observed to be narrow and sharp indicating its crystalline nature. The peaks were sharper and narrower in C-ZrP and chromium loaded C-ZrP suggesting increase in crystallinity due to the presence of ZrP and chromium further suggesting that ZrP was well dispersed onto chitosan network though crystallinity was reasonably retained as also evidenced by TEM figures in CZrP and Cr-C-ZrP.

3.3.8. ESR Analysis

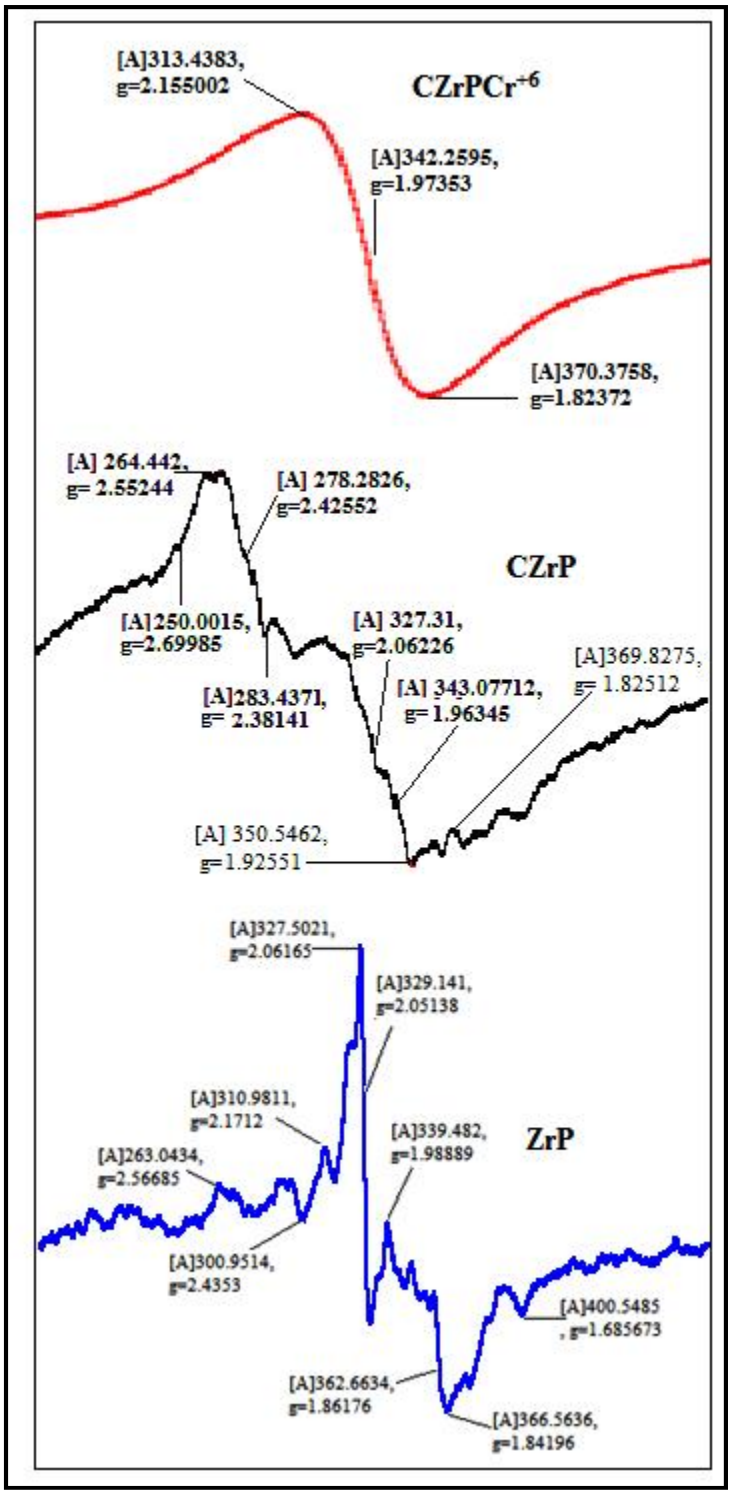

Figure 3.10 ESR of a) ZrP, b) CZrP and c) CZrPCr

Figure 3.10 shows the ESR spectra of ZrP and CZrP. In ZrP the signal at 1.988 is attributed to Zr^{3+} while the signal at 2.051 and 2.061 is attributed to zirconium superoxide radical anions ($Zr^{4+}(O-\bullet\ ^{2}$), while the peak at g 1.861 is attributed to F-center localized near

Zr^{4+} ion (D.L. Griscom & Friebele, 1991; David L Griscom, 1993). The g value at 1.86 eV for ZrP can be attributed to F center near Zr^{4+} ion/Zr^{3+} present as defects in ZrP which should contain Zr^{4+} ions and g value of 2.05 can be attributed to O_2^- peroxy radical which stabilizes the Zr^{3+} ion. (Giamello, Volante, Fubini, Geobaldo, & Morterra, 1991).

The use of autoclave generated defects in zirconium phosphate.EPR spectroscopy is reported to be one of the most suitable techniques to investigate defects in materials (Dyrek & Che, 1997). However such defects are not reported in zirconium phosphate.

Autoclaving at high temperatures could create both oxygen vacancies and electrons. There must be loss of water molecules, hydroxyl groups and even lattice oxygen that will leave oxygen vacancies in ZrP. In the absence of oxygen in the gas phase, the electrons in excess will be trapped forming Zr^{3+}, or in the oxygen vacancies giving a signal .

In CZrP the signal at 1.963 is attributed to Zr^{3+} while the signal at 2.062 is attributed to zirconium superoxide radical anions ($Zr^{4+}(O-\bullet\ 2)$). The signal at 1.963can be also attributed to Zr^{3+} in tetragonally compressed octahedron (Aboukaïs et al., 2002). 1.825 and 1.925 F center near Zr. g value of 2.062 can be attributed to O_2^- peroxy radical which stabilizes the Zr^{3+} ion. The CZrP sample possessed various signals characteristic of paramagnetic centers. The peroxy radical can be identified in CZrP also with its characteristic signal at 2.06eV and Zr^{3+} contributes to the signal at 1.963.

In Cr-CZrP the signal at 1.973 is attributed to Zr^{3+} or Cr^{3+}. The broad peak at 1.973 can be attributed to Cr^{3+} clusters. This signal could also be attributed to F+ center surrounded by zirconium ions .

3.3.9 XPS Analysis

Figure 3.11 shows the wide scan spectra of ZrP and CZrP

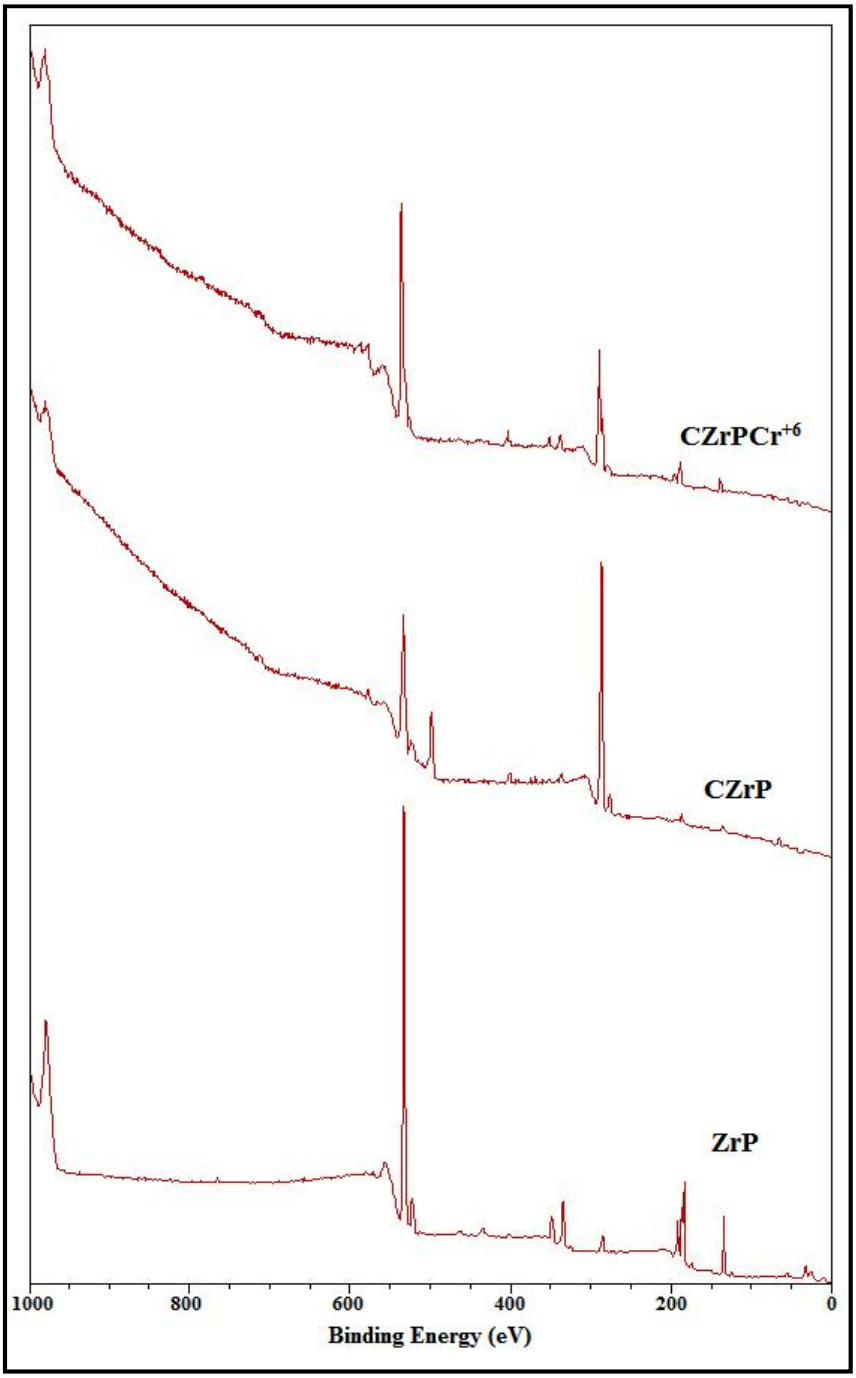

Figure 3.11 XPS of a) ZrP, b) CZrP and c) CZrPCr

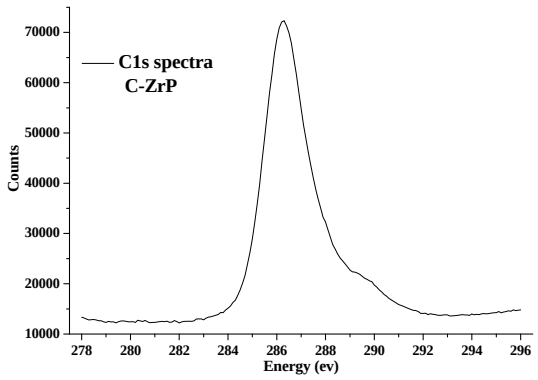
C1s spectra
C-ZrP
Counts
Energy (ev)

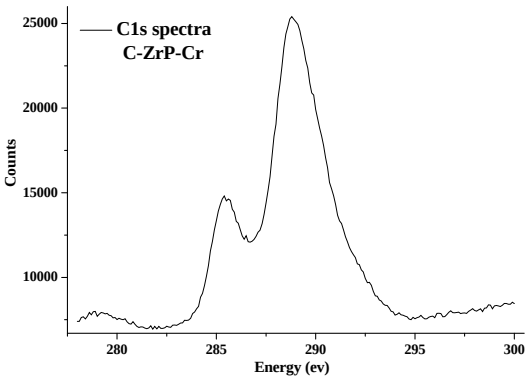
C1s spectra
C-ZrP-Cr
Counts
Energy (ev)

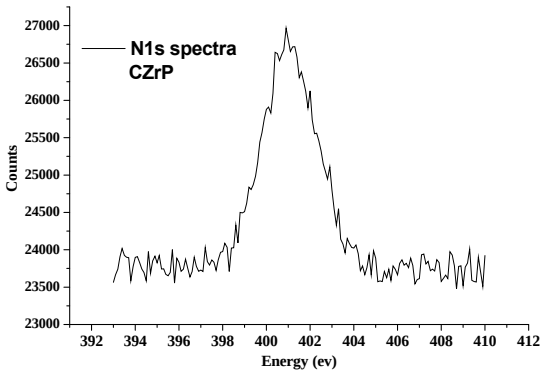
N1s spectra
CZrP
Counts
Energy (ev)

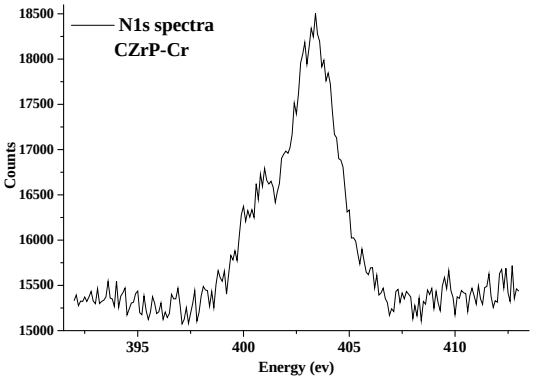
N1s spectra
CZrP-Cr
Counts
Energy (ev)

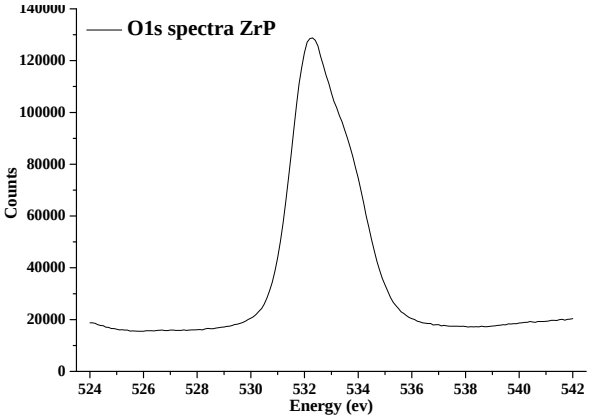
O1s spectra ZrP
Counts
Energy (ev)

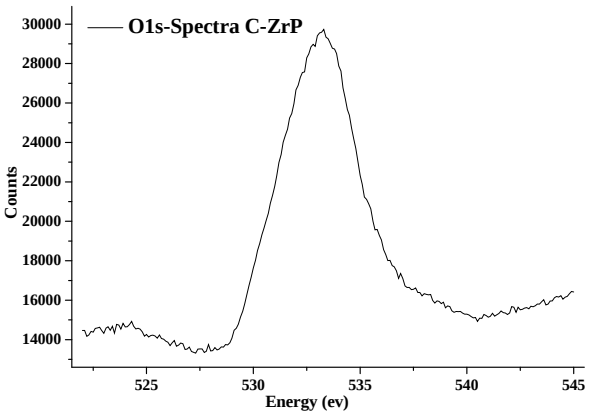
O1s-Spectra C-ZrP
Counts
Energy (ev)

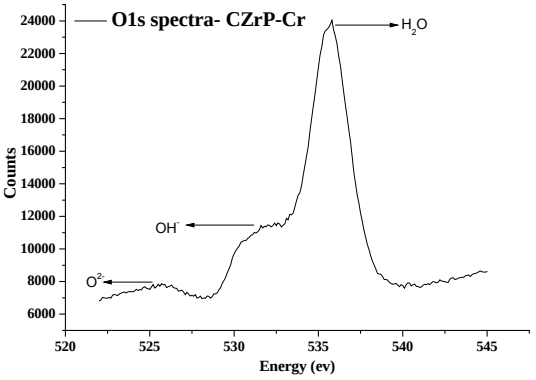
O1s spectra- CZrP-Cr
H2O
OH-
O2-
Counts
Energy (ev)

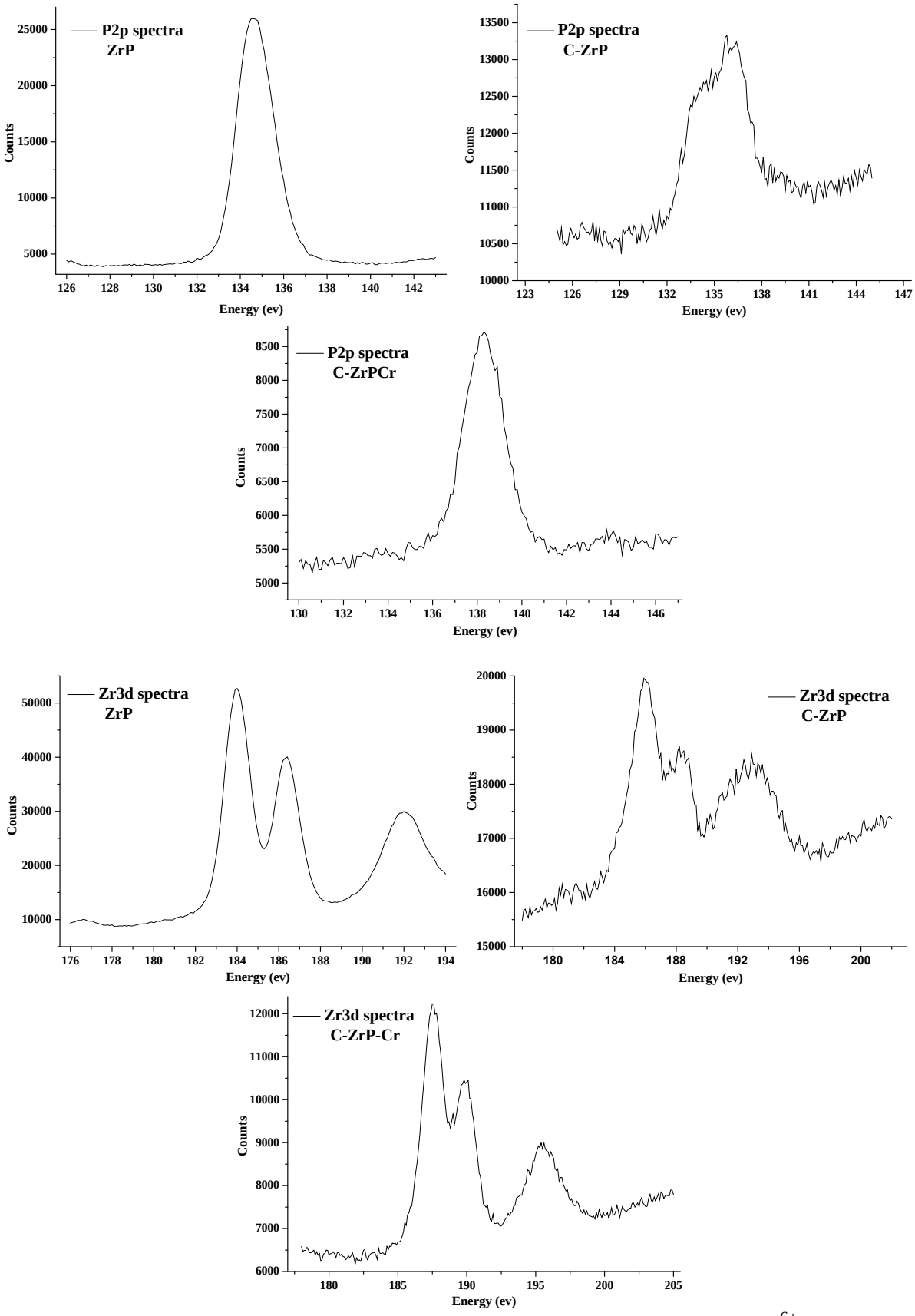

Figure 3.12 Deconvoluted xps spectra for ZrP, CZrP and CZrP-Cr^{6+}

Table 3.4 XPS assignment

Compound	Atom	Binding Energy (ev)	Assignment
ZrP	O1s	530.5	O=P
	O1s	531.4	O–Zr, O-P, Zr-OH, P-OH
	O1s	532.3	physisorbed water
	P2p	134	characteristic of P^{5+}
	$Zr3d_{5/2}$	183.9	Zr4+
	$Zr3d_{3/2}$	186.4	Zr^{4+}
	$Zr3d_{5/2}$	178.6	Zr^{3+}
	$Zr3d_{3/2}$	180.2	Zr^{3+}
CZrP	O1s	533	broad peak
	P2p	133.6	characteristic of P^{5+}
	P2p	136.4	polyphosphate
	$Zr3d_{5/2}$	186.1	Zr4+
	$Zr3d_{3/2}$	188.2	Zr^{4+}
	N1s	397.31	N-H+
	N1s	400.1	N-Zr
	N1s	397.2	C-N
	N1s	400.9	NH3+
CZrPCr	O1s	535	broad peak
	P2p	132.9	characteristic of P^{5+}
	P2p	138.3	polyphosphate
	$Zr3d_{5/2}$	187.5	Zr4+
	$Zr3d_{3/2}$	189.5	Zr^{4+}
	N1s	400.9	C-N
	N1s	401	NH_3^+
	$Cr2p_{3/2}$	576.7, 586.7	Cr^{3+}
	$Cr2p_{1/2}$	580, 589.2	Cr^{6+}

Figure 3.12 shows the XPS spectra of O 1s , which fits well with three peaks at 530.5, 531.4 and 532.3 eV in ZrP. The first peak at 530.5 eV was assigned to double-bonded oxygen with phosphorus.. The second peak (531.4 eV) represents the oxygen im O–P and O–Zr that overlaps with the binding energies of Zr–OH and P–OH. The third peak, at higher binding energy of 532.8 eV, can be attributed to physisorbed water. In CZrP and CZrP-Cr the oxygen peaks could not be deconvoluted and broad peaks with binding energy of 533 and 535 eV for CZrP and CrCZrP respectively are observed

The P 2p binding energy in ZrP is observed at 134 eV, which is characteristic of P^{5+} (Splinter, Rofagha, McIntyre, & Erb, 1996). The P 2p binding energies are observed at133.6eV and 136.4eV in CZrP which can be attributed to P^{5+} and polyphosphate

respectively The small peak at 132.9 in CZrP-Cr can be attributed to P^{5+}. The binding energy peak at 138.3 eV is attributed to polyphosphate.

For Zr the characteristic 3d doublets were observed. The binding energy peaks at 183.9 eV &186.4eV , 186.1& 188.2, 187.5& 189.5 are attributed to 3d5/2 $Zr^{4+}$and 3d3/2 $Zr^{4+}$of ZrP, CZrP and CZrP-Cr respectively may be attributed to fully oxidised Zr^{4+} state of zirconium while the lower binding energy peaks at 178.6/180.2 eV in ZrP to Zr^{3+} The peaks were observed to be broader in CZrP indicating the polycrystalline nature (Jang et al., 2013).

N states at 397.31 eV and 400.1eV are observed in the spectrum of CZrP. These arise from coordination between N and H^+ and N-Zr , respectively. On adsorption of Cr four peaks are observed for N indicating change in coordination environment

In CZrP the biding energies of 397.2eV and 400.9eV are attributed to C-N and NH_3^+. The peak at 400.9eV shifted to 401 as a small shoulder suggesting that although reduction of Cr^{6+} to Cr^{3+} occurred on surface of CZrP , the main adsorption mechanism for Cr^{6+} onto CZrP was based on ionic interaction(Ren et al., 2016).

The Binding energies of 576.7 and 586.7 eV corresponded to Cr^{3+} while binding energies of 580 and 589.2 eV corresponded to Cr^{6+} (Cr2p3/2 and Cr2p½ orbitals respectively) in CZrP-Cr.

3.4 ADSORPTION-DESORPTION STUDIES

3.4.1 Effect of pH

pH has a very significant effect in determining Cr^{6+} biosorption on ZrP-chitosan composite. Cr^{6+} adsorption on ZrP-chitosan as a function of pH is shown in Figure 3.13. The maximum adsorption capacity was found in the pH range 3-5. At low pH, dominant form of Cr^{6+} is $HCrO_4^-$ which was exchanged with H^+ of CZrP

$$HCrO_4^- \leftrightarrow CrO_4^{2-} + H^+, \quad pK_a = 5.9$$

$$H_2CrO_4 \leftrightarrow CrO_4^- + H^+, \quad pK_a = 4.1$$

$$Cr_2O_7^{2-} + H_2O \leftrightarrow 2HCrO_4^-, \quad pK_a = 2.2$$

However, at pH greater than 6 chromium removal capacity of CZrP was found to decrease. The decrease of chromium uptake at neutral / basic pH conditions may be due to competition for active cationic site bindings by presence of excessive hydroxyl anions (Figure 3.13).

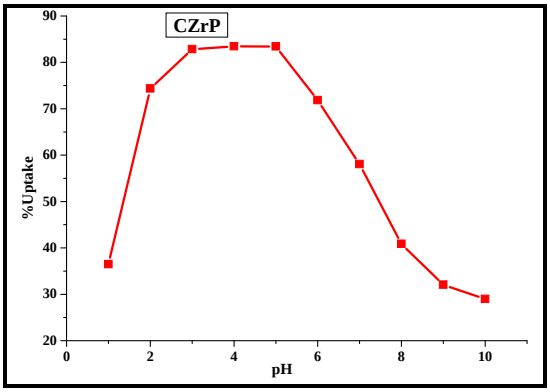

Figure 3.13 Effect of pH :

Volume = 25 ml, Amount adsorbent = 0.05 g, [Cr^{6+}] = 50 ppm: pH = 1 to 10, contact time =4 h, Temp. Temp.= 30°C.

3.4.2 Effect of Adsorbent Dose

When the dose of C-ZrP was increased from 0.05 g to 0.1 g/L the % removal of Cr^{6+} increased linearly and a plateau was obtained at 0.07 g probably due to unavailability of Cr^{6+} in the solution for more and more adsorption sites of incoming adsorbent. Thus, beyond 0.07 g/L of C-ZrP , there was no remarkable change in removal efficiency of Cr^{6+}.

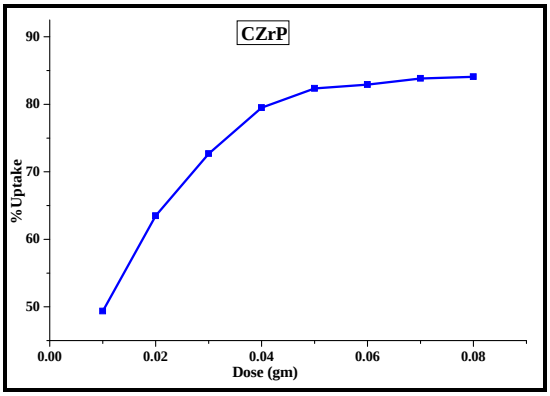

Figure 3.14 Effect of Dose

Volume = 25 ml, Amount adsorbent = 0.05 g to 0.1g, [Cr^{6+}] = 50ppm : pH = 3, contact time =4 h, Temp. = 30°C.

3.4.3 Effect of Concentration Variation

The uptake of chromium was found to decrease with increase in concentration of CZrP (Figure 3.15), suggesting that limiting number of adsorption sites were available for adsorption as concentration of adsorbate molecules increased.

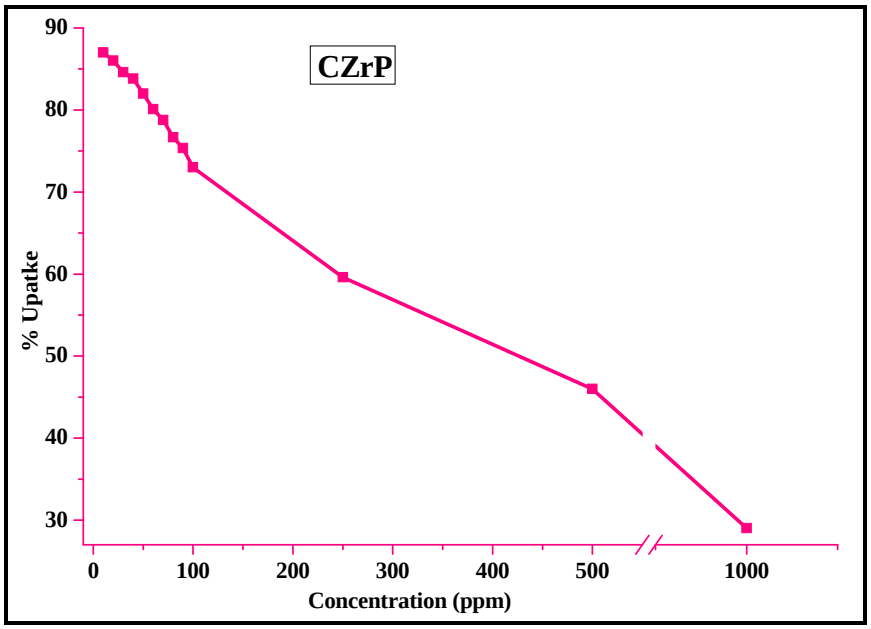

Figure 3.15 Concentration Variation

Volume = 25 ml, Amount adsorbent = 0.05g, [Cr^{6+}] = 50ppm to 1000ppm : pH = 4, contact time =4 h, Temp. = 30°C.

To verify the adsorption mechanism, the adsorption isotherm of CZrp was fitted with different isotherm models (Chapter 2 and Section 2.2.5) and isotherm constants calculated for the adsorption of Cr^{6+} by adsorbent are presented in Table 3.5. The Freundlich constant, n was more than unity implying the effective interaction between Cr^{6+} and heterogeneous surface of CZrP and hence favorable adsorption. The maximum adsorption capacity was calculated using Langmuir isotherm model and was found to be 155.52mg.g^{-1}. The fitting of Temkin model indicated favorable adsorption of Cr^{6+} onto adsorbent under study. From Temkin model, typical bonding energy range for the ion exchange mechanism was reported to be in the range of 8– 16 kJ mol^{-1} while the physisorption process was reported to have adsorption energies less than −40 kJ mol^{-1} . The value of B_T (31.21 kJ mol^{-1}) obtained in the present study indicated that the adsorption process seemed to be involve both physisorption and chemisorption. The high regression values for Halsey model suggest multilayer adsorption. However the negative nH values and low values of Kh suggest that the model is not a good fit to describe the adsorption process. The flory Huggins model was seen to fit the adsorption data well indicating monolayer adsorption involving functional groups. The fitting of Elovich model further affirmed that the adsorption process was predominantly chemisorption.

Table 3.5 Isotherm Parameters

Model	**Constants**				
Freundlich	K_f (L.g^{-1})	N	r^2	SD	
	9.1212	2.5942	0.9899	0.031	
Langmuir	K_L(L.mmol^{-})	qm (mg.g-1)	ΔG(kJ.mol^{-1})	r2	SD
	0.0145	155.52	-10.9951	0.99	0.1347
Halsey	k_H (L.g-1)	nH	r2	SD	
	0.754	-1.882	0.9943	0.0529	
Temkin	BT	-ΔH (kJ.mol^{-1})	K_T (L.mmol^{-1})	r^2	SD
	31.2186	12.5495	0.136	0.9913	4.8097
F-H	nfh	Kfh	r2	SD	
	-0.093	-0.093	0.9994	0.0013	
Elovich	qm (mg.g-1)	Lnqm	K_E (L.mmol^{-1})	r^2	SD
	0.0184	-3.9948	2.9E+29	0.9885	4.7661

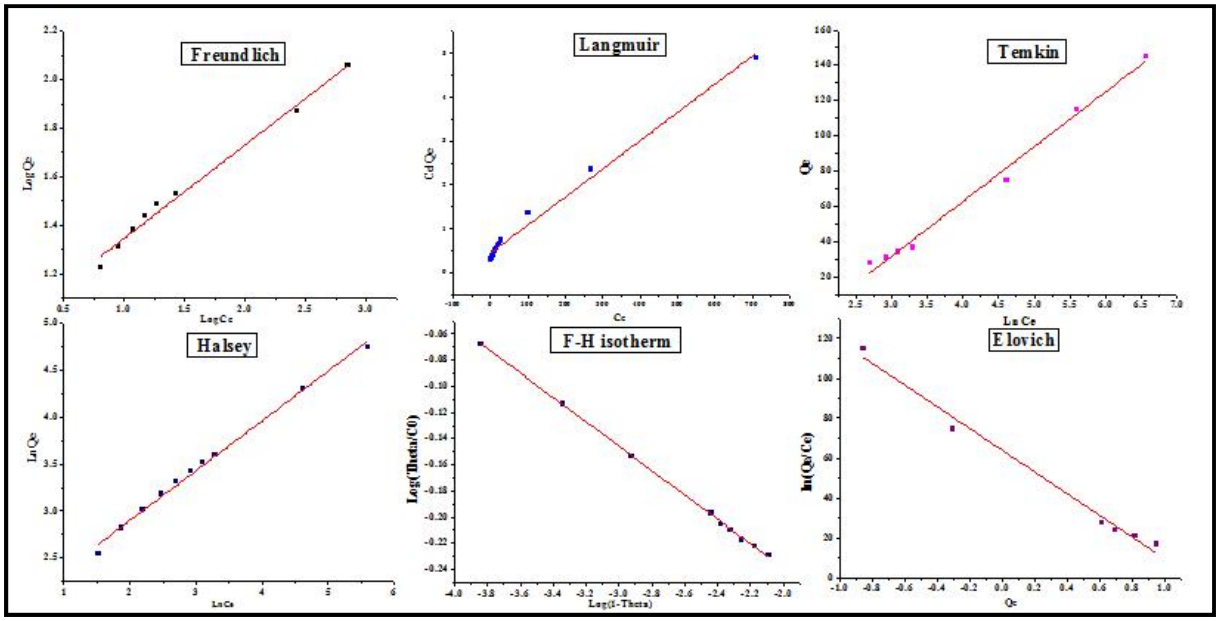

Figure 3.16 Linear fit of Isotherm

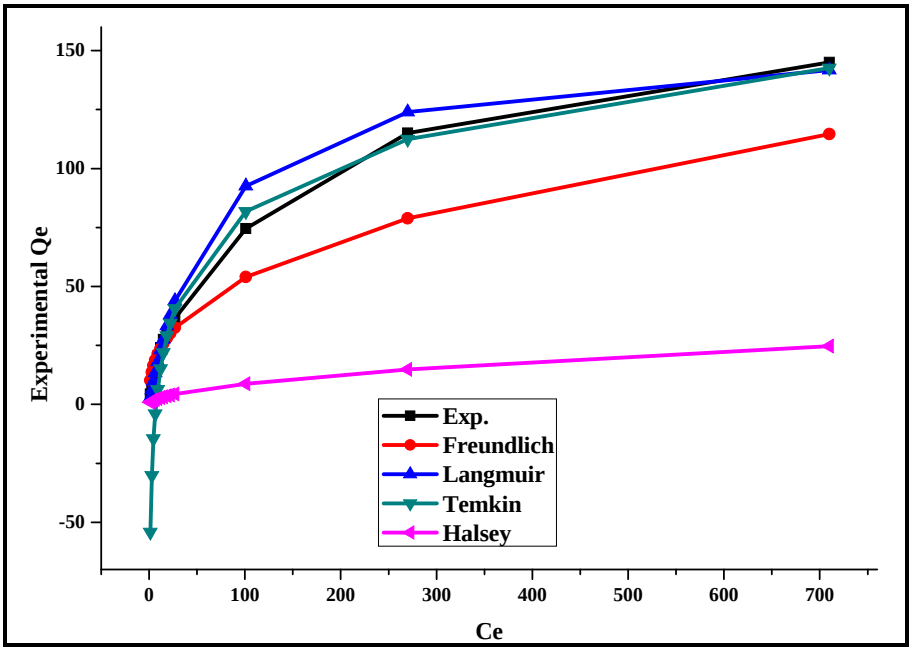

Figure 3.17 Isotherm model fitting for CZrP

3.4.7 Sorption Kinetics

The effect of contact time for adsorption of Cr^{6+} onto CZrP is depicted in figure - 3.18. It was observed that the initial rate of adsorption of Cr^{6+} onto CZrP was fast with an uptake of about ~80% in first 60 min and further reached equilibrium in 120 min. The removal rate is high initially due to the presence of free binding sites on layers of CZrP which gradually become filled with chromium ions with time. Afterwards the filling of vacant sites became difficult due to repulsive forces between chromium ions on CZrP surface and solution (Ma et al., 2016b).

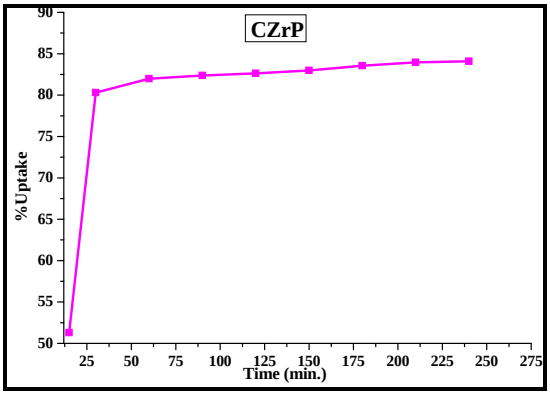

Figure 3.18 Effect of Time

Volume = 25 ml, Amount adsorbent = 0.05 g, [Cr^{6+}] = 50 ppm : pH = 4, contact time=4 h, Temp. = 30°C.

To evaluate the adsorption kinetics, different kinetic models were applied, and fitting results are shown in figure 3.19 and the rate constants for the adsorption of Cr^{+6} by adsorbent

are presented in Table 3.6 to get further insight into adsorption kinetics of Cr^{6+} onto CZrP.All the models under study gave reasonably good correlation coefficients and the calculated equilibrium adsorption capacity values were closer to those obtained experimentally for pseudo second order model. This supported the assumption behind the model that the chemisorption may be the rate-limiting step.

The Elovich kinetic model was fitted with good correlation coefficient. The initial adsorption rate, α, and the desorption constant, β, were calculated from slope and intercept of straight line plot between Qt and ln(t) for CZrP. The constant β related to the extension of surface coverage was found to be very low indicating that uptake of chromium onto CZrP may have been more through functional groups. However, the constant α that is related to chemisorption rate was high suggesting that more than one mechanism governs the uptake of chromium. The large α values as compared to β suggested that the rate of adsorption was much higher than the rate of desorption indicating the high feasibility of adsorption process.

The non-zero intercept of the linear plot of q_t versus $t^{1/2}$ in IP as well as in LFD models indicated that diffusion is not the only rate-limiting step but may also be influenced by external mass transfer of Cr^{6+} from solution phase to solid phase, pore diffusion and further to interior sites of the adsorbent. Thus the adsorption of Cr^{6+} by CZrP was controlled by boundary layer as well as diffusion process The reasonably good correlation coefficient for Bangham equation indicated that the diffusion of Cr^{6+} into the pores of the adsorbents under study also controlled the adsorption process. It was thus concluded that the metal adsorption process was controlled by more than one step. The uptake kinetics can thus be controlled by different diffusion steps: (a) bulk diffusion from aqueous solution, film (or external) diffusion, and intraparticle diffusion as well as diffusion into pores of the adsorbent; apart from interaction of chromium with CZrP (chemisorption) that may contribute to the control of mass transfer (Krys et al., 2013).

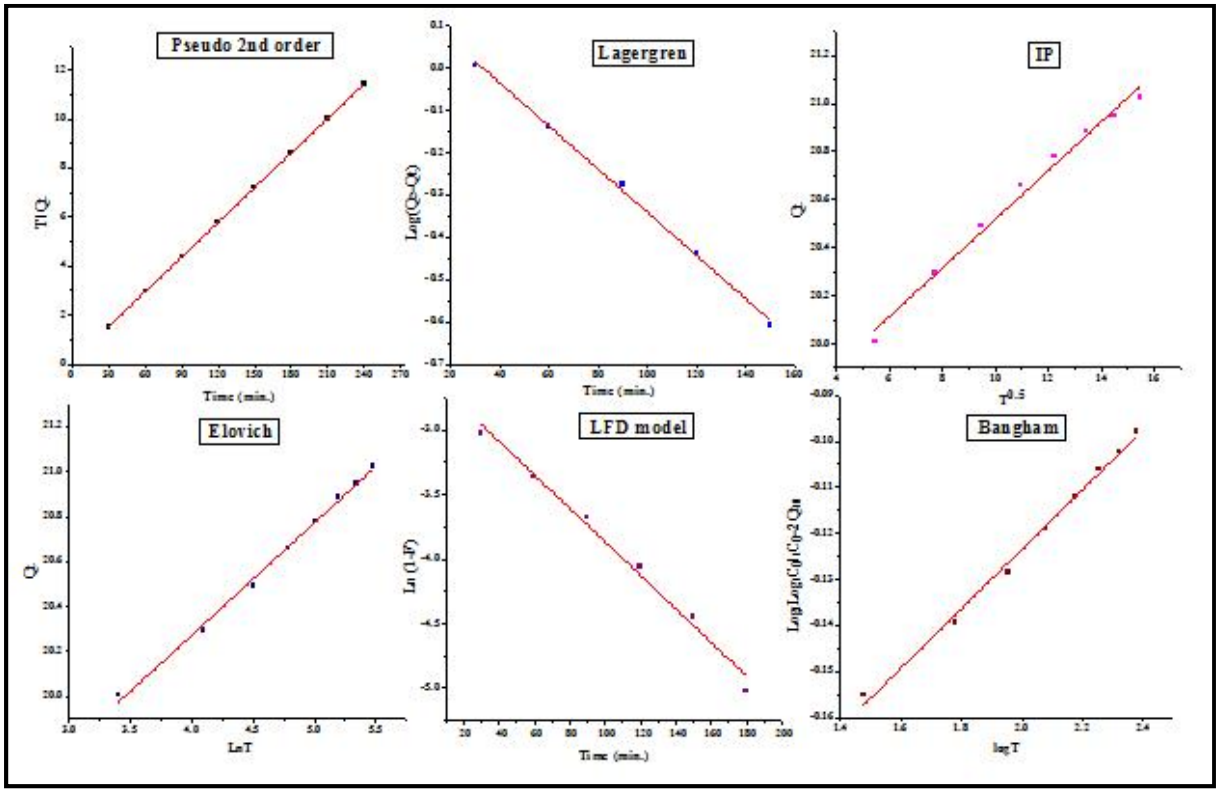

Figure 3.19 Linear fit of Kinetics for CZrP

Table 3.6 Kinetic Parameters for Cr^{6+} loaded CZrP

Model	**Constants**				
Pseudo second order	q_t (mg/g)	K	r^2	H	SD
	21.204 (q_t exp. 21.023 mg/g)	0.0178	0.9998	8.0019	0.0257
Lagergren	q_e (mg/g)	K	r^2	SD	
	1.4763	0.0118	0.9978	0.0131	
IP	K	I	r^2	SD	
	0.1013	19.505	0.9882	0.0410	
Elovich	B	Alpha	r^2	SD	
	2.0092	2.7E+36	0.9964	0.0229	
Liquid film diffusion model	K_{fd}	r^2	SD		
	0.0129	0.9882	0.0885		
Bangham	K_m	Alpha	r^2	SD	
	-14.561	0.0647	0.9948	0.0015	

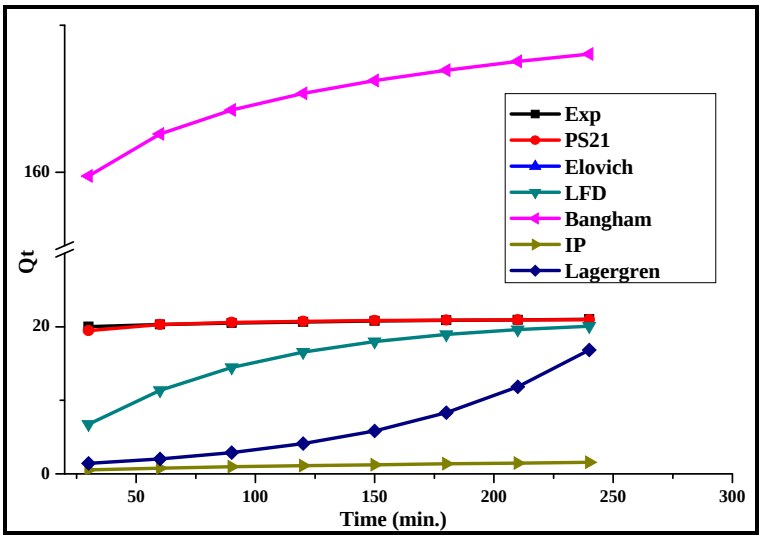

Figure 3.20 Kinetics Back Calculation for CZrP

3.4.5 Effect of Temperature.

The chromium uptake on CZrP decreased with increase in temperature from 30 to 70°C (Figure 3.21) indicating that the adsorption process was exothermic. (Pandey & Mishra, 2011).

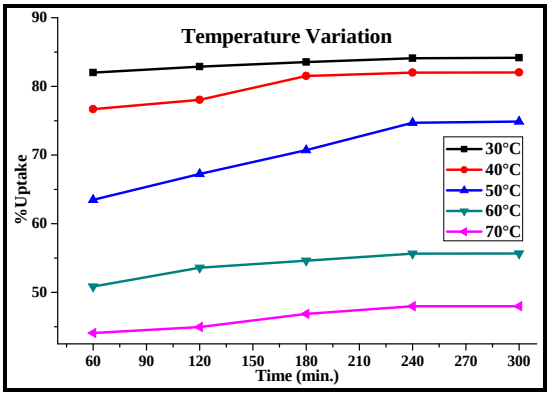

Figure 3.21 Temperature Variation

Volume = 25 ml, Amount adsorbent = 0.05 g, [Cr^{6+}] = 50 ppm effect of temperature: pH = 4, contact time =1-4 h, Temp. = 30-70°C.

Thermodynamic parameters of the adsorption process when determined from the experimental data revealed that the free energy change during the adsorption process was negative for the experimental range of temperatures (Table 3.7) and less than -10KJ/ mol suggesting chemisorption to be the mechanism of adsorption. The negative value of enthalpy change indicated that the adsorption was physical in nature involving strong forces of attraction and is exothermic. The negative entropy change corresponded to decrease in the degree of freedom of the adsorbed species.

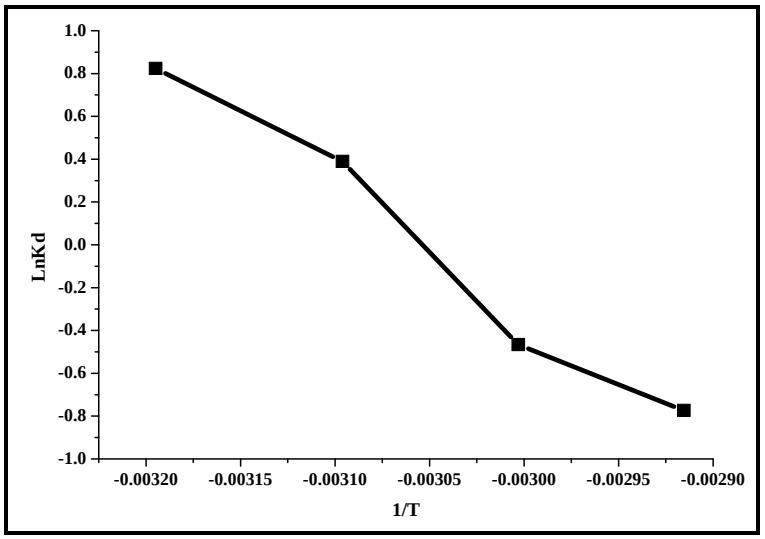

Figure 3.22 Thermodynamics plot

Table 3.7 Thermodynamic parameters

Temp K	ΔG kJ/mole	ΔH kJ/mole	ΔS J/moleK
303	-3.774	-50.4584	-154.0738
313	-2.2333		
323	-0.6926		
333	0.8482		
343	2.3889		

3.4.6 Desorption and reuse of adsorbents

It is observed from Figure 3.23 that maximum desorption of chromium (87%) occurred in 0.1 N NaOH solution. This could be attributed to competition of OH^- ions with $HCrO_4^-$on treatment with NaOH solution. Furthermore, it was also observed that chromium was not desorbed as Cr^{6+} (negligible color with diphenylcarbazide) but as Cr^{3+} affirming the fact that Cr^{6+} was almost completely converted into Cr^{3+} on CZrP. After desorption CZrP was reused up to four adsorption desorption cycles and the results are presented in Figure 3.24. It was found that the adsorption capacity of the CZrP decreased by 33% after first cycle, 10% after 2nd cycle and 29% after the third cycle The removal displayed a decrease in efficiency after each cycle probably because all active sites within ZrP cannot be regenerated readily by NaOH solution. Similar observation was made by Zhang et al during their investigation of removal of phosphate using ZrP (Q. Zhang et al., 2013) .

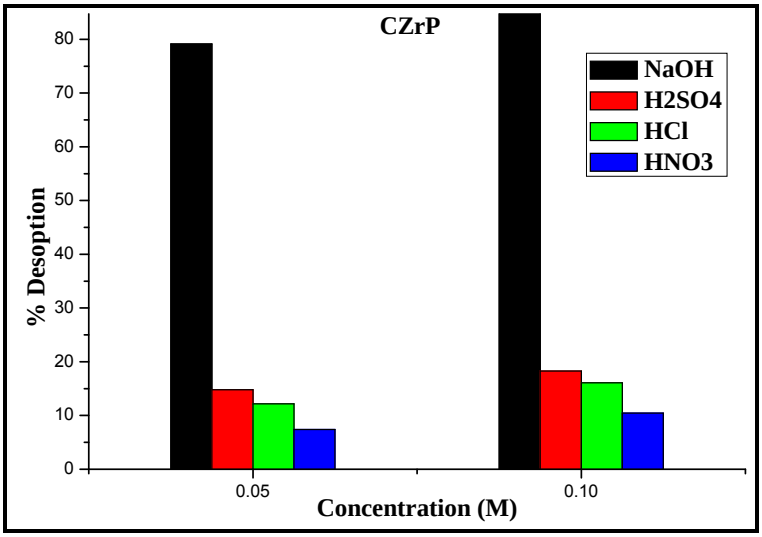

Figure 3.235 % Desorption for CZrP

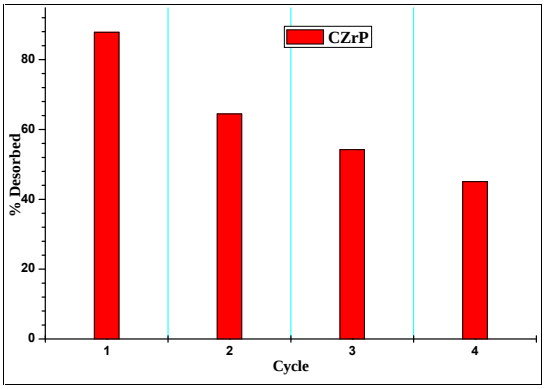

Figure 3.246 %Desorption for 3 cycles for CZrP

3.7 Mechanism

The possible mechanism for the removal of chromium is by ion exchange mechanism as shown in Fig. 3.25 An ion exchange mechanism is involved as with exchangeable protons of ZrP and also hydrogen bonding herefore, it was deduced that the main mechanisms of chromium adsorption on CZrP should be controlled by hydrogen bonding (physical adsorption) and ion exchange reactions (chemical adsorption) . This was followed by reduction of Cr^{6+} to Cr^{3+} and coordinative binding of Cr^{3+} to ZrP

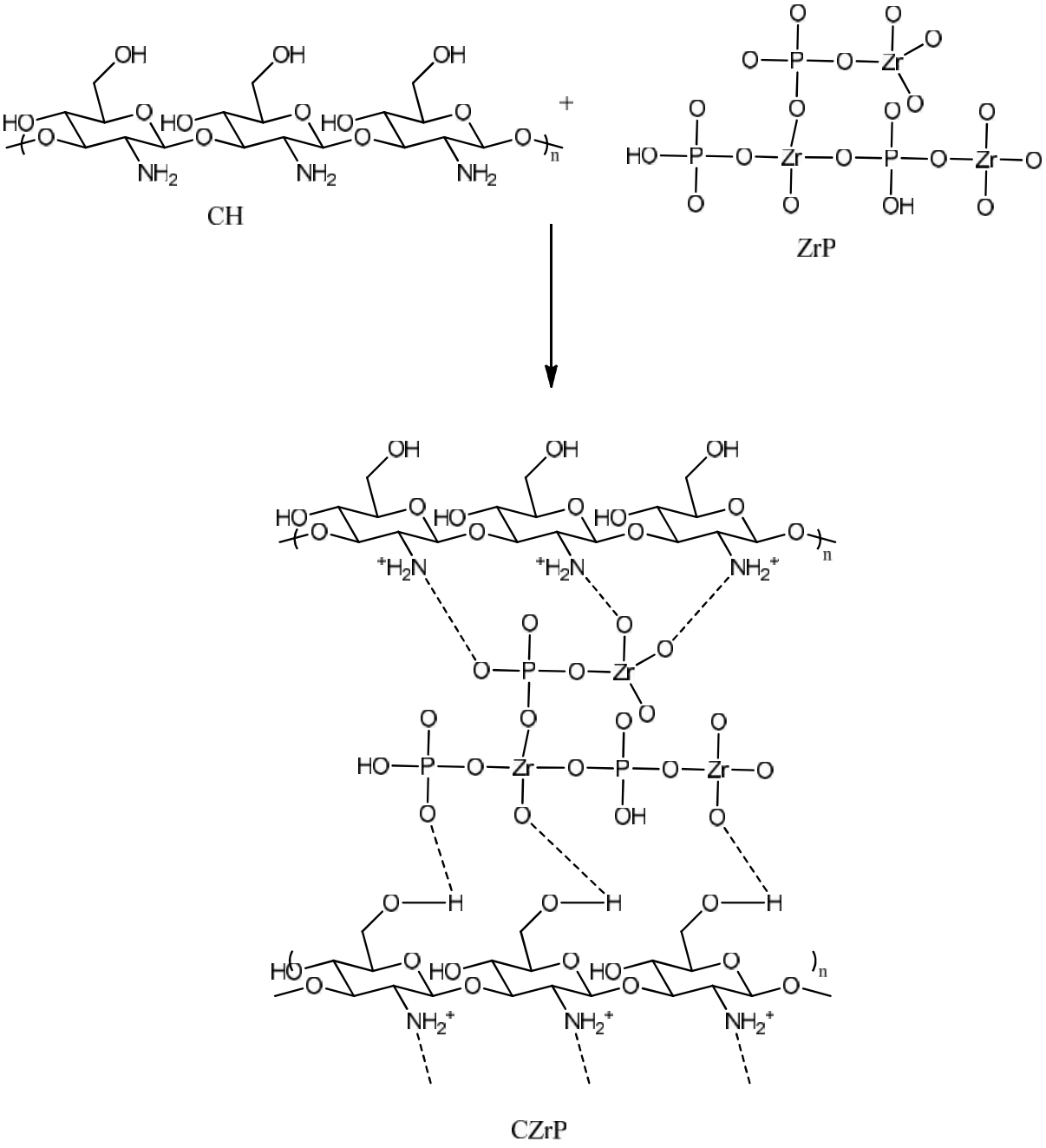

Figure 3.25 CH, ZrP and CZrP

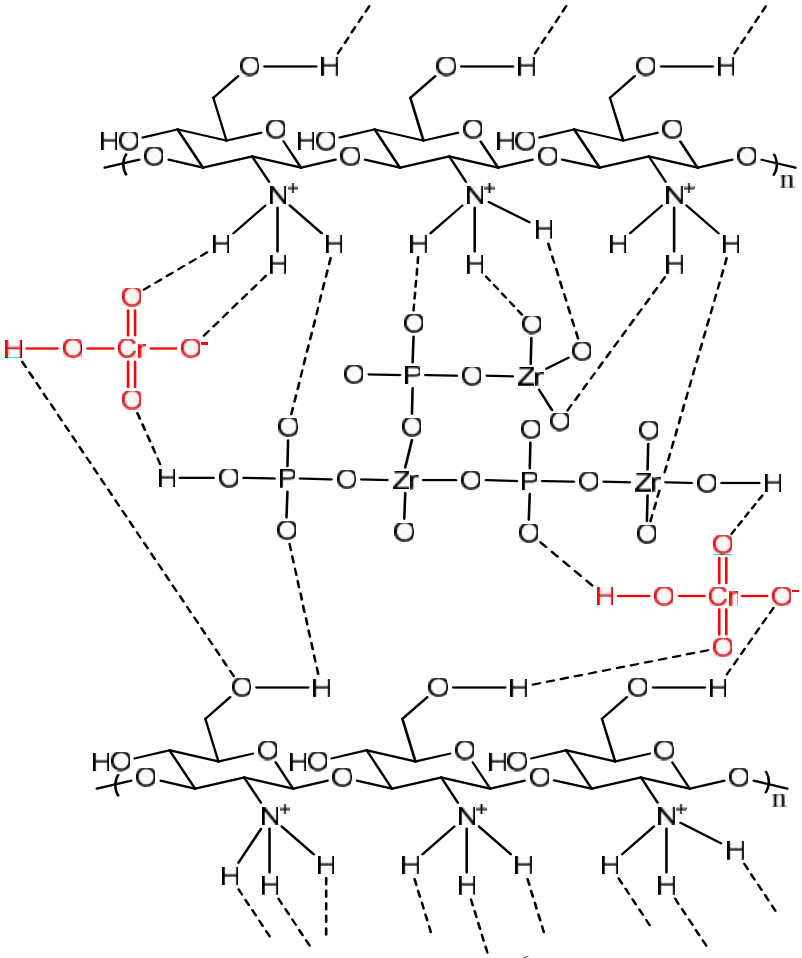

Figure 3.26 $CZrPCr^{6+}$

3.6 Conclusion

Literature reveals chitosan-derivative sorbents were used for removal of cations, due to free electron lone pairs in O and N-atoms of chitosan linkage. Thus, metals like zirconium (IV) get attached at primary –NH and OH groups of chitosan due to electrostatic attraction. This metal doped chitosan cationic site with exchangeable H^+ ions is vital in chromate anion sorption mechanism. Equilibrium solution pH had a remarkable effect on chromium adsorption capacity. pH 4.0 was found to be optimum for the maximum removal of chromium metal. Among the kinetic models tested, the adsorption kinetics was best described by the pseudo-second-order equation. The data fitted well with the Langmuir adsorption isotherm model.

Biosorbent displayed a surface controlled adsorption, indicating a monolayer sorption by interactions between chromate anion and zirconium doped chitosan. Adsorption thermodynamics indicate the adsorption process of chromium onto CZrP was exothermic.

3.7 References

Aboukaïs, A., Bogomolova, L. D., Deshkovskaya, A. A., Jachkin, V. A., Krasil'nikova, N. A., Prushinsky, S. A., … Zhilinskaya, E. A. (2002). {EPR} of silica and fluoride glasses implanted with titanium and zirconium. *Optical Materials*, *19*(2), 295–306. doi:http://dx.doi.org/10.1016/S0925-3467(01)00226-9

Abutartour, A., Jia, Y., Majdoub, L. El, & Xu, Q. (2014). A new hierarchical porous zirconium phosphate membrane and its adsorption properties. *Microporous and Mesoporous Materials*, *196*, 1–7. doi:10.1016/j.micromeso.2014.04.054

Anirudhan, T. S., Bringle, C. D., & Radhakrishnan, P. G. (2012). Heavy metal interactions with phosphatic clay: Kinetic and equilibrium studies. *Chemical Engineering Journal*, *200-202*, 149–157. doi:10.1016/j.cej.2012.06.024

Cabatingan, L. K., Agapay, R. C., Rakels, J. L. L., Ottens, M., & van der Wielen, L. a. M. (2001). Potential of Biosorption for the Recovery of Chromate in Industrial Wastewaters. *Industrial & Engineering Chemistry Research*, *40*(10), 2302–2309. doi:10.1021/ie0008575

Cai, X., Dai, G. J., Tan, S. Z., Ouyang, Y., Ouyang, Y. S., & Shi, Q. S. (2012). Synergistic antibacterial zinc ions and cerium ions loaded??-zirconium phosphate. *Materials Letters*, *67*(1), 199–201. doi:10.1016/j.matlet.2011.09.041

Calogero, S., Lanari, D., Orr??, M., Piermatti, O., Pizzo, F., & Vaccaro, L. (2011). Supported l-proline on zirconium phosphates methyl and/or phenyl phosphonates as heterogeneous organocatalysts for direct asymmetric aldol addition. *Journal of Catalysis*, *282*(1), 112–119. doi:10.1016/j.jcat.2011.06.004

Chakravarty, R., Ram, R., Pillai, K. T., Pamale, Y., Kamat, R. V., & Dash, A. (2012). Ammonium molybdophosphate impregnated alumina microspheres as a new generation sorbent for chromatographic 137Cs/137mBa generator. *Journal of Chromatography A*, *1220*, 82–91. doi:10.1016/j.chroma.2011.11.059

Chang, C. Y., Chau, L. K., Hu, W. P., Wang, C. Y., & Liao, J. H. (2008). Nickel hexacyanoferrate multilayers on functionalized mesoporous silica supports for selective sorption and sensing of cesium. *Microporous and Mesoporous Materials*, *109*(1-3), 505–512. doi:10.1016/j.micromeso.2007.05.057

Chauhan, D., Jaiswal, M., & Sankararamakrishnan, N. (2012). Removal of cadmium and hexavalent chromium from electroplating waste water using thiocarbamoyl chitosan. *Carbohydrate Polymers*, *88*(2), 670–675. doi:10.1016/j.carbpol.2012.01.014

Chourasia, R., Bohre, A., Shrivastava, O. P., & Wattal, P. . (2010). Crystallographic evaluation of sodium zirconium phosphate as a host structure for immobilization of cesium and strontium. *International Journal of Applied Ceramic Technology*, *45*, 533–545. doi:10.1111/j.1744-7402.2012.02811.x

Chowdhury, S. R., Yanful, E. K., & Pratt, A. R. (2012). Chemical states in XPS and Raman analysis during removal of Cr(VI) from contaminated water by mixed maghemite-magnetite nanoparticles. *Journal of Hazardous Materials*, *235-236*, 246–256. doi:10.1016/j.jhazmat.2012.07.054

Clearfield, A., & Smith, G. D. (1969). Crystallography and structure of .alpha.-zirconium bis(monohydrogen orthophosphate) monohydrate. *Inorganic Chemistry*, *8*(3), 431–436. doi:10.1021/ic50073a005

Clearfield, A., & Stynes, J. A. (1964). The Preparation of Ccrystalline Zirconium Phosphate and Some Observations on Its Ion Exchange Behaviour. *Journal of Inorganic and Nuclear Chemistry*, *26*(1), 117–129. doi:http://dx.doi.org/10.1016/0022-1902(64)80238-4

Dongre, R., Ghugal, D. N., Meshram, J. S., & Ramteke, D. S. (2012). Fluoride removal from water by zirconium (IV) doped chitosan bio-composite. *African Journal of Environmental Science and Technology*, *6*(2), 130–141. doi:10.5897/AJEST11.284

Du, X., Zhang, Q., Qiao, W., Sun, X., Ma, X., Hao, X., … Guan, G. (2016). Controlled self-assembly of oligomers-grafted fibrous polyaniline/single zirconium phosphate nanosheet hybrids with potential-responsive ion exchange properties. *Chemical Engineering Journal*, *302*, 516–525. doi:http://dx.doi.org/10.1016/j.cej.2016.05.066

Dyrek, K., & Che, M. (1997). EPR as a Tool To Investigate the Transition Metal Chemistry on Oxide Surfaces. *Chemical Reviews*, *97*(1), 305–332. doi:10.1021/cr950259d

Elovich, S. Y., & Larionov, O. . (1962). Theory of adsorption from nonelectrolyte solutions on solid adsorbents. *Russian Chemical Bulletin*, *11*(2), 191–197.

Giamello, E., Volante, M., Fubini, B., Geobaldo, F., & Morterra, C. (1991). Workshop on Clusters and Surfaces An EPR study on the formation of the superoxide radical ion on monoclinic zirconia. *Materials Chemistry and Physics*, *29*(1), 379–386. doi:http://dx.doi.org/10.1016/0254-0584(91)90032-P

Griscom, D. L. (1993). Proceedings of the Eight International Symposium on Halide Glasses Defect centers in heavy-metal fluoride glasses: a review. *Journal of Non-Crystalline Solids*, *161*, 45–51. doi:http://dx.doi.org/10.1016/0022-3093(93)90667-M

Griscom, D. L., & Friebele, E. J. (1991). *Fluoride Glass Fiber Optic*. (I. Aggarwal & G. Lu, Eds.). Academic Press, Boston.

He, J., Li, Y., Xue, X., Ru, H., Huang, X., & Yang, H. (2016). Separation of fluorine/cerium from fluorine-bearing rare earth sulfate solution by selective adsorption using hydrous zirconium oxide. *RSC Advances*, *6*(49), 43814–43822. doi:10.1039/c6ra03590f

Hei, Y. ., & Ma, H. . (2016). The adsorption of Cr(III) in tanning wastewater by Zr-MMT nanomaterial. *Journal of Fucntional Materials*, *47*, 51–55.

Hepplewhite, C., Newcombe, G., & Knappe, D. R. U. (2004). NOM and MIB, who wins in the competition for activated carbon adsorption sites? *Water Science and Technology*, *49*(9), 257–265.

Hosseini, S. F., Rezaei, M., Zandi, M., & Farahmandghavi, F. (2015). Preparation and Characterization of Chitosan Nanoparticles-Loaded Fish Gelatin-Based Edible Films. *Journal of Food Process Engineering*. doi:10.1111/jfpe.12246

Jaimez, E., Khainakov, S. A., Trobajo, C., & Rodrı, J. (1998). Synthesis of New n -Alkylamines Intercalation Compounds with r -Titanium Phosphate . Process Characterization. *Chemistry of Materials*, *4756*(12), 2490–2496.

Jang, I. H., Um, S. H., Lim, B., Woo, M. H., Jun, K.-W., Lee, J.-B., & Bae, J. W. (2013). Effects of surface modification with zirconium phosphate on Ru/Co/SiO2 Fischer–Tropsch catalysts analyzed by {XPS} and {TEM} analyses. *Applied Catalysis A: General*, *450*, 88–95. doi:http://dx.doi.org/10.1016/j.apcata.2012.10.020

Jiang, H., Chen, P., Luo, S., Tu, X., Cao, Q., & Shu, M. (2013). Synthesis of novel nanocomposite Fe3O4/ZrO2/chitosan and its application for removal of nitrate and phosphate. *Applied Surface Science*, *284*, 942–949. doi:10.1016/j.apsusc.2013.04.013

Karlsson, M., Andersson, C., & Hjortkjaer, J. (2001). Hydroformylation of propene and 1-hexene catalysed by a α-zirconium phosphate supported rhodium-phosphine complex. *Journal of Molecular Catalysis A: Chemical*, *166*(2), 337–343. doi:10.1016/S1381-1169(00)00480-5

Kousalya, G. N., Rajiv Gandhi, M., & Meenakshi, S. (2010). Sorption of chromium(VI) using modified forms of chitosan beads. *International Journal of Biological Macromolecules*, *47*(2), 308–315. doi:10.1016/j.ijbiomac.2010.03.010

Krys, P., Testa, F., Trochimczuk, A., Pin, C., Taulemesse, J. M., Vincent, T., & Guibal, E. (2013). Encapsulation of ammonium molybdophosphate and zirconium phosphate in alginate matrix for the sorption of rubidium(I). *Journal of Colloid and Interface Science*,

409, 141–150. doi:10.1016/j.jcis.2013.07.046

Kumada, N., Hinata, J., Dong, Q., Yonesaki, Y., Takei, T., & Kinomura, N. (2011). Preparation and crystal structure of two types of zirconium phosphates by hydrothermal reaction. *Journal of the Ceramic Society of Japan*, *119*(1390), 412–416. doi:10.2109/jcersj2.119.412

Liu, Q., Hu, P., Wang, J., Zhang, L., & Huang, R. (2016). Phosphate adsorption from aqueous solutions by Zirconium (IV) loaded cross-linked chitosan particles. *Journal of the Taiwan Institute of Chemical Engineers*, *59*, 311–319. doi:10.1016/j.jtice.2015.08.012

Liu, X., & Zhang, L. (2015). Removal of phosphate anions using the modified chitosan beads: Adsorption kinetic, isotherm and mechanism studies. *Powder Technology*, *277*, 112–119. doi:10.1016/j.powtec.2015.02.055

Ma, H., Hei, Y., Hua, L., Guo, Y., Yang, Y., Yu, C., & Qiao, X. (2016a). Fabrication of zirconium-pillared montmorillonite porous ceramic as adsorbents for Cr3+ removal and recycling. *Ceramics International*, *42*(13), 14903–14909. doi:10.1016/j.ceramint.2016.06.130

Ma, H., Hei, Y., Hua, L., Guo, Y., Yang, Y., Yu, C., & Qiao, X. (2016b). Fabrication of zirconium-pillared montmorillonite porous ceramic as adsorbents for Cr3+ removal and recycling. *Ceramics International*, *42*(13), 14903–14909. doi:http://dx.doi.org/10.1016/j.ceramint.2016.06.130

Maltez, H. F., & Carasek, E. (2005). Chromium speciation and preconcentration using zirconium(IV) and zirconium(IV) phosphate chemically immobilized onto silica gel surface using a flow system and F AAS. *Talanta*, *65*(2), 537–542. doi:10.1016/j.talanta.2004.07.017

Mao, J.-G., Wang, Z., & Clearfield, A. (2002). New lead inorganic-organic hybrid microporous and layered materials: synthesis, properties, and crystal structures. *Inorganic Chemistry*, *41*(23), 6106–11. Retrieved from http://www.ncbi.nlm.nih.gov/pubmed/12425639

Mathew, A. P., & Dufresne, A. (2002). Morphological Investigation of Nanocomposites from Sorbitol Plasticized Starch and Tunicin Whiskers. *Biomacromolecules*, *3*(3), 609–617. doi:10.1021/bm0101769

Matoso, E., Kubota, L. T., & Cadore, S. (2003). Use of silica gel chemically modified with zirconium phosphate for preconcentration and determination of lead and copper by

flame atomic absorption spectrometry. *Talanta*, *60*(6), 1105–1111. doi:10.1016/S0039-9140(03)00215-7

Mimura, H., Wu, Y., Yufei, W., Niibori, Y., Yamagishi, I., Ozawa, M., … Koyama, S. (2011). Selective separation and recovery of cesium by ammonium tungstophosphate-alginate microcapsules. In *Nuclear Engineering and Design* (Vol. 241, pp. 4750–4757). doi:10.1016/j.nucengdes.2011.03.031

Mosby, B. M., Díaz, A., Bakhmutov, V., & Clearfield, A. (2014). Surface functionalization of zirconium phosphate nanoplatelets for the design of polymer fillers. *ACS Applied Materials and Interfaces*, *6*(1), 585–592. doi:10.1021/am4046553

Murray, H. H. (2006). *Applied Clay Mineralogy: Occurrences, Processing and Applications of Kaolins, Bentonites, Palygorskite-Sepiolite, and Common Clays* (1st ed.).

Nilchi, A., Zarghami, R., Saberi, R., Moradi, M., & Azizpour, H. (2012). Evaluation of AMP-PAN composite for adsorption of Cs + ions from aqueous solution using batch and fixed bed operations. *Journal of Radioanalytical and Nuclear Chemistry*, *291*(2), 609–617. doi:10.1007/s10967-011-1455-6

Nishiyama, N., Nishiyama, Y., Tanaka, S., Hillhouse, H. W., Egashira, Y., & Ueyama, K. (2006). Synthesis of ordered mesoporous zirconium phosphate films by spin coating and vapor treatments. *Langmuir*, *22*(23), 9469–9472. doi:10.1021/la061493+

Pan, B. C., Zhang, Q. R., Zhang, W. M., Pan, B. J., Du, W., Lv, L., … Zhang, Q. X. (2007). Highly effective removal of heavy metals by polymer-based zirconium phosphate: A case study of lead ion. *Journal of Colloid and Interface Science*, *310*(1), 99–105. doi:10.1016/j.jcis.2007.01.064

Pan, B., Pan, B., Chen, X., Zhang, W., Zhang, X., Zhang, Q., … Chen, J. (2006). Preparation and preliminary assessment of polymer-supported zirconium phosphate for selective lead removal from contaminated water. *Water Research*, *40*(15), 2938–2946. doi:10.1016/j.watres.2006.05.028

Pan, B., Zhang, Q., Du, W., Zhang, W., Pan, B., Zhang, Q., … Zhang, Q. (2007). Selective heavy metals removal from waters by amorphous zirconium phosphate: Behavior and mechanism. *Water Research*, *41*(14), 3103–3111. doi:10.1016/j.watres.2007.03.004

Pandey, S., & Mishra, S. B. (2011). Organic-inorganic hybrid of chitosan/organoclay bionanocomposites for hexavalent chromium uptake. *Journal of Colloid and Interface Science*, *361*(2), 509–520. doi:10.1016/j.jcis.2011.05.031

Pathania, D., Sharma, G., & Thakur, R. (2015). Pectin @ zirconium (IV) silicophosphate

nanocomposite ion exchanger: Photo catalysis, heavy metal separation and antibacterial activity. *Chemical Engineering Journal*, *267*, 235–244. doi:10.1016/j.cej.2015.01.004

Pica, M., Donnadio, A., Capitani, D., Vivani, R., Troni, E., & Casciola, M. (2011). Advances in the chemistry of nanosized zirconium phosphates: A new mild and quick route to the synthesis of nanocrystals. *Inorganic Chemistry*, *50*(22), 11623–11630. doi:10.1021/ic2015594

Ren, Z., Xu, X., Wang, X., Gao, B., Yue, Q., Song, W., … Wang, H. (2016). FTIR, Raman, and XPS analysis during phosphate, nitrate and Cr(VI) removal by amine cross-linking biosorbent. *Journal of Colloid and Interface Science*, *468*, 313–323. doi:10.1016/j.jcis.2016.01.079

Rudzinski, W., & Panczyk, T. (2002). The Langmuirian adsorption kinetics revised: A farewell to the XXth century theories? *Adsorption*, *8*(1), 23–34. doi:10.1023/A:1015214406179

Satyanarayana, J., Murthy, G. S., & Sasidhar, P. (1999). Adsorption studies of cesium on a new inorganic exchanger ammonium molybdophosphate - Alumina (AMP - Al2O3). *Journal of Radioanalytical and Nuclear Chemistry*, *242*(1), 11–16. doi:10.1007/BF02345888

Sowmya, A., & Meenakshi, S. (2014). Zr(IV) loaded cross-linked chitosan beads with enhanced surface area for the removal of nitrate and phosphate. *International Journal of Biological Macromolecules*, *69*, 336–343. doi:10.1016/j.ijbiomac.2014.05.043

Splinter, S. J., Rofagha, R., McIntyre, N. S., & Erb, U. (1996). XPS Characterization of the Corrosion Films Formed on Nanocrystalline Ni-P Alloys in Sulphuric Acid. *Surface and Interface Analysis*, *24*(3), 181–186. doi:10.1002/(SICI)1096-9918(199603)24:3<181::AID-SIA92>3.0.CO;2-N

Sun, L., Boo, W. J., Browning, R. L., Sue, H. J., & Clearfield, A. (2005). Effect of crystallinity on the intercalation of monoamine in??-zirconium phosphate layer structure. *Chemistry of Materials*, *17*(23), 5606–5609. doi:10.1021/cm051160i

Swain, S. K., Patnaik, T., Singh, V. K., Jha, U., Patel, R. K., & Dey, R. K. (2011). Kinetics, equilibrium and thermodynamic aspects of removal of fluoride from drinking water using meso-structured zirconium phosphate. *Chemical Engineering Journal*, *171*(3), 1218–1226. doi:10.1016/j.cej.2011.05.030

Sydorchuk, V., Khalameida, S., Skubiszewska-Zieba, J., & Leboda, R. (2011). Synthesis and structure of AMP/oxide support. *Journal of Thermal Analysis and Calorimetry*, *103*(1),

257–265. doi:10.1007/s10973-010-0967-6

Takei, T., Kobayashi, Y., Hata, H., Yonesaki, Y., Kumada, N., Kinomura, N., & Mallouk, T. E. (2006). Anodic electrodeposition of highly oriented zirconium phosphate and polyaniline-intercalated zirconium phosphate films. *Journal of the American Chemical Society*, *128*(51), 16634–16640. doi:10.1021/ja065677m

Tranter, T. J., Herbst, R. S., & Todd, T. A. (2002). Determination of a solid phase mass transfer coefficient for modeling an adsorption bed system using ammonium molybdophosphate-polyacrylonitrile (AMP-PAN) as a sorbent for the removal of 137Cs from acidic nuclear waste solutions. *Adsorption*, *8*(4), 291–299. doi:10.1023/A:1021533429787

Trobajo, C., Khainakov, S. A., Espina, A., García, J. R., Salvadó, M. A., Pertierra, P., … Bortun, A. I. (2001). Synthesis of a mineral - Organic hybrid by treatment of phlogopite with phenylphosphonic acid. *Chemistry of Materials*, *13*(12), 4457–4462. doi:10.1021/cm011005d

Troup, J. M., & Clearfield, A. (1977). Mechanism of ion exchange in zirconium phosphates. 20. Refinement of the crystal structure of .alpha.-zirconium phosphate. *Inorganic Chemistry*, *16*(12), 3311–3314. doi:10.1021/ic50178a065

Wang, J. S., Peng, R. T., Yang, J. H., Liu, Y. C., & Hu, X. J. (2011). Preparation of ethylenediamine-modified magnetic chitosan complex for adsorption of uranyl ions. *Carbohydrate Polymers*, *84*(3), 1169–1175. doi:10.1016/j.carbpol.2011.01.007

Wang, L., Xu, W. H., Yang, R., Zhou, T., Hou, D., Zheng, X., … Huang, X. J. (2013). Electrochemical and density functional theory investigation on high selectivity and sensitivity of exfoliated nano-zirconium phosphate toward lead(II). *Analytical Chemistry*, *85*(8), 3984–3990. doi:10.1021/ac3037014

Waraich, S. M. Biomimetic Fabrication of Organic-Inorganic Composite Materials (2012). Retrieved from https://www.google.co.in/url?sa=t&rct=j&q=&esrc=s&source=web&cd=1&cad=rja&uact=8&ved=0ahUKEwjY-J3G4NDOAhVLuY8KHZxzDSUQFggiMAA&url=http://digisrv-1.biblio.etc.tu-bs.de:8080/docportal/servlets/MCRFileNodeServlet/DocPortal_derivate_00023076%2

Weckhuysen, B. M., & Schoonheydt, R. a. (1999). Olefin polymerization over supported chromium oxide catalysts. *Catalysis Today*, *51*, 215–221. doi:10.1016/S0920-5861(99)00046-2

Wu, H., Liu, C., Chen, J., Chang, P. R., Chen, Y., & Anderson, D. P. (2009). Structure and properties of starch/α-zirconium phosphate nanocomposite films. *Carbohydrate Polymers*, *77*(2), 358–364. doi:10.1016/j.carbpol.2009.01.002

Wu, Z., Zhang, L., Guan, Q., Ning, P., & Ye, D. (2014). Preparation of α-zirconium phosphate-pillared reduced graphene oxide with increased adsorption towards methylene blue. *Chemical Engineering Journal*, *258*, 77–84. doi:10.1016/j.cej.2014.07.064

Yan-Qing, W., Zhao-Jia, L., & Ming-Lin, G. (2015). Hydrothermal synthesized microflower sodium zirconium phosphate and its transformation to zirconium hydrogen phosphate. *Materials Letters*, *159*, 197–199. doi:http://dx.doi.org/10.1016/j.matlet.2015.06.114

Zhang, F., Xie, Y., Lu, W., Wang, X., Xu, S., & Lei, X. (2010). Preparation of microspherical α-zirconium phosphate catalysts for conversion of fatty acid methyl esters to monoethanolamides. *Journal of Colloid and Interface Science*, *349*(2), 571–577. doi:10.1016/j.jcis.2010.05.043

Zhang, Q., Du, Q., Jiao, T., Pan, B., Zhang, Z., Sun, Q., … Gao, F. (2013). Selective removal of phosphate in waters using a novel of cation adsorbent: Zirconium phosphate (ZrP) behavior and mechanism. *Chemical Engineering Journal*, *221*, 315–321. doi:10.1016/j.cej.2013.02.001

Zhang, Q., Jiang, P., Pan, B., Zhang, W., & Lv, L. (2009). Impregnating zirconium phosphate onto porous polymers for lead removal from waters: Effect of nanosized particles and polymer chemistry. *Industrial and Engineering Chemistry Research*, *48*(9), 4495–4499. doi:10.1021/ie8016847

Zhang, Q., Pan, B., Zhang, S., Wang, J., Zhang, W., & Lv, L. (2011). New insights into nanocomposite adsorbents for water treatment: A case study of polystyrene-supported zirconium phosphate nanoparticles for lead removal. *Journal of Nanoparticle Research*, *13*(10), 5355–5364. doi:10.1007/s11051-011-0521-x

Zhao, D., Li, F. F., Zhang, A. Y., Yang, L., & Zhu, R. (2011). CsAlZr2(PO4)4: An anhydrous aluminium zirconium phosphate with a novel three-dimensional framework. *Acta Crystallographica Section C: Crystal Structure Communications*, *67*(1), 4–6. doi:10.1107/S0108270110050535

Zhao, D., Yu, Y., & Chen, J. P. (2016). Treatment of lead contaminated water by a PVDF membrane that is modified by zirconium, phosphate and PVA. *Water Research*, *101*, 564–573. doi:10.1016/j.watres.2016.04.078

Zhao, H., Li, N., Li, J., Qiao, X., & Xu, Z. (2015). Preparation and Application of Chitosan-

Grafted Multiwalled Carbon Nanotubes in Matrix Solid-Phase Dispersion Extraction for Determination of Trace Acrylamide in Foods Through High-Performance Liquid Chromatography. *Food Analytical Methods*, *8*(5), 1363–1371. doi:10.1007/s12161-014-0022-5

Zhu, H. Y., Jiang, R., Xiao, L., & Zeng, G. M. (2010). Preparation, characterization, adsorption kinetics and thermodynamics of novel magnetic chitosan enwrapping nanosized γ-Fe2O3 and multi-walled carbon nanotubes with enhanced adsorption properties for methyl orange. *Bioresource Technology*, *101*(14), 5063–5069. doi:http://dx.doi.org/10.1016/j.biortech.2010.01.107

Zuo, X., & Balasubramanian, R. (2013). Evaluation of a novel chitosan polymer-based adsorbent for the removal of chromium (III) in aqueous solutions. *Carbohydrate Polymers*, *92*(2), 2181–2186. doi:10.1016/j.carbpol.2012.12.009